CR-111843

THE PENNSYLVANIA
STATE UNIVERSITY

A NUMERICAL SOLUTION OF THE UNSTEADY AIRFOIL WITH APPLICATION TO THE VORTEX INTERACTION PROBLEM

By

Wylie E. Rudhman

December 1970

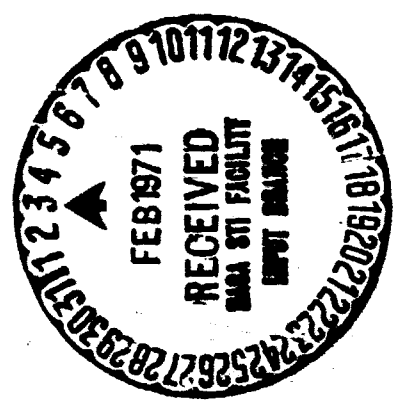

DEPARTMENT OF AEROSPACE ENGINEERING

UNIVERSITY PARK, PENNSYLVANIA

ABSTRACT

A numerical method to predict the aerodynamic forces acting on a thin airfoil operating in an unsteady potential flow is developed. A distribution of discrete point vortices placed on an arbitrary camber line represents the airfoil. The time dependent solution including wake generation is obtained starting with the system at rest. A rigid wake assumption is used where the wake vortices lie in the direction of the chord line and move with the free stream velocity. The results of the numerical solution are shown to agree with results using the classic theories of Theodorsen for the oscillating airfoil and of Wagner for the impulsively started airfoil.

Using the numerical method, a parametric study is conducted to determine the time history of the loads on an airfoil produced by a vortex passing in proximity to the airfoil. Results of the study are compared to an experimental investigation of the rotor blade-vortex interaction problem, but agreement was not obtained. The general trends of the experimental parameters are confirmed by the theory, but the magnitudes of the fluctuating blade loads are overestimated. Satisfactory agreement is obtained, however, by correcting the two-dimensional results for finite aspect ratio effects using the Prandtl tip loss factor.

TABLE OF CONTENTS

ACKNOWLEDGMENTS

The author wishes to extend sincere thanks to his advisor, Professor Barnes W. McCormick, Jr., for his time, technical assistance and patience in the preparation of this thesis. In addition, the tolerance of Mr. Gerald F. Hall to many questions and arguments is greatly appreciated.

This study was sponsored by the National Aeronautics and Space Administration (Langley) Contract No. NGR 39-009-111, and is gratefully acknowledged.

NOMENCLATURE

a	Position of axis of rotation, defined in Figure 1.
b	Airfoil semichord length.
c	Airfoil chord length.
C(k)	Theodorsen function, F(k) + i G(k).
C_ℓ	Section lift coefficient, $\ell/(1/2\ \rho\ V^2\ c)$.
ΔC_ℓ	Maximum difference in C_ℓ in a vortex sweep.
$C_{\ell ss}$	Section steady state lift coefficient.
C_m	Section moment coefficient.
h	Distance of vortex above or below airfoil.
h'	Coordinate of blade motion in vertical direction.
i,j,k	Summation indices.
k	Reduced frequency, w b/V.
ℓ	Section lift.
m	Number of time increments.
n	Number of vortices on airfoil.

s	Distance traveled in semichords.
t,Δt	Time and time increment.
ΔT	Time interval between positive and negative peak C_ℓ values in vortex interaction.
V	Free stream velocity.
V_r	Resultant velocity due to vortex and free stream.
V_x	Horizontal component of V_r
x_v	Horizontal distance of vortex from airfoil leading edge.

Greek

α	Angle of attack of airfoil.
α_v	Vortex induced angle of attack.
β	Phase angle for steady state approximation to oscillating airfoil.
δ	Intersection angle of blade and vortex.
$\gamma(x)$	Distributed bound vortex strength per unit length.
$\Gamma(m)$	Circulation at time m.
Γ_v	Strength of passing vortex.
ω	Frequency of oscillation

ξ Control point location on airfoil.

ρ Fluid density.

ϕ Phase angle for unsteady solution to oscillating airfoil.

$\phi(s)$ Wagner function.

LIST OF FIGURES

I. INTRODUCTION

The interaction of an aerodynamic surface with a vortex is of current interest for two reasons. First, the flight of a light aircraft into the wake of a heavier one can be hazardous. Uncontrollable rolling moments can be experienced when flying parallel to a trailing vortex and severe turbulence is experienced when flying through the vortex perpendicular to the axis. The second reason concerns the noise and blade stresses produced during helicopter operations. A helicopter blade can intersect the trailing vortex shed by another blade causing a rapid fluctuation in the blade loads. This intersection is known to be the source of the familiar blade slap noise.

The present study is concerned with the airfoil-vortex interaction problem. A numerical technique using discrete vortices is developed to predict the forces acting on a two-dimensional thin airfoil in the unsteady flow produced by a vortex passing close to the airfoil. The usual restrictions of potential flow are imposed on the problem.

The computational model consists of a number of bound vortices placed on the mean camber line of the airfoil section and shed vortices starting from the trailing edge and lying in the wake in

the direction of the chord line. The unsteady problem starts from rest. At each time increment the airfoil sheds a vortex at the trailing edge which moves downstream with the velocity of the free stream. The airfoil-vortex interaction problem is modeled by placing a potential vortex in the flow upstream of the airfoil. This vortex then moves downstream past the airfoil as time progresses. The vortex moves with the free stream velocity and the induced velocities of the bound and shed vortices. Figure 1 illustrates the problem and defines the coordinates.

The digital computer program used in the study is written in Fortran IV language and appears in the appendix. An IBM 360/67 computer was used for the calculations.

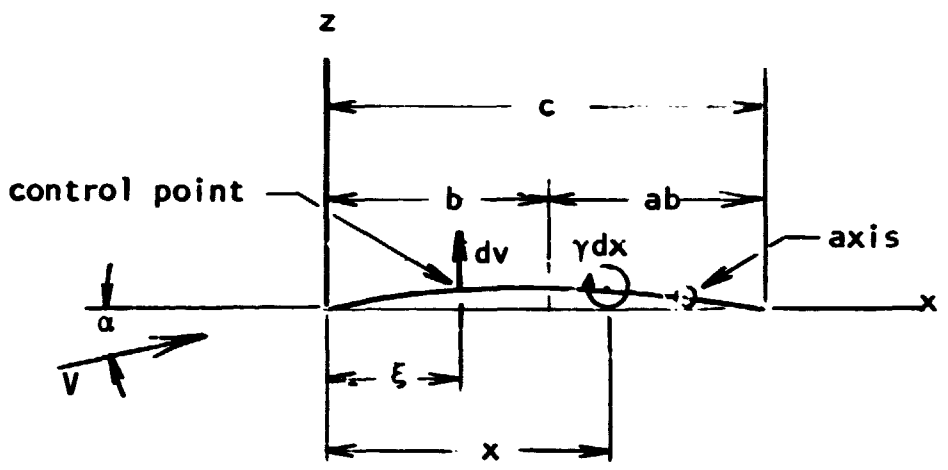

Figure 1 Definition of Coordinates

II. PREVIOUS INVESTIGATION

The objective of the present study was to develop a method using two-dimensional thin airfoil theory to predict the time history of the forces on a rigid helicopter blade operating in the influence of a vortex. The first step was to develop a numerical procedure to accurately describe the unsteady aerodynamics of the blade itself operating in some time-dependent flow field. A model capable of producing a detailed chordiwise pressure distribution and capable of generating its own wake from the start of the problem was formulated. To select such a model the work of others in numerical unsteady aerodynamics was reviewed.

Two-dimensional, unsteady aerodynamics with linearized equations has been considered in detail by the classic methods of Theodorsen[18], von Karman[10] and Sears[14]. The nonlinear effects of thickness and wake distortion have been accounted for by Giesing[5] using a distribution of doublets on an airfoil. Giesing has solved the problem numerically and has found the nonlinearities to act in general to retard any change in the lift. The experimental results of Spurck[16] for airfoil oscillations in a wind tunnel confirm Giesings' results and show that the real fluid effects also retard the lift build-up. A detailed

discussion of the deforming wake as it applies to the present study is discussed in Section III. The three-dimensional problem of a wing moving unsteadily in a potential flow has been solved by Djojodihardjo and Widnall[3]. A numerical solution to an integral equation representation of the wing and wake is given including thickness and wake roll-up effects.

The proper numerical generation of the shed vortex wake has been investigated by Piziali[13]. Normally, a wake is generated by sheding a vortex into the wake at each time increment where the first and each new vortex is formed slightly downstream of the trailing edge. If the distance from the trailing edge of the shed vortex is equal to the wake element spacing, $V\Delta t$, in the limit of infinitesimal time increments, the wake is continuous and emerges from the trailing edge as a sheet. Piziali, however, has found a model which advances the wake toward the trailing edge by an amount equal to 7/10 of the wake element spacing to give the best results when compared to the Theodorsen function for an oscillating airfoil. For the advanced wake, the first and each newly shed vortex appears 3/10 of the spacing downstream. This somewhat artificial representation of the wake has not been used in the present study.

The effects of wing (or helicopter blade) and vortex interaction

has been the subject of a considerable amount of recent research[7,8,9,11,15,17,19]. Theoretical studies have been made with varying degrees of simplification and experimental investigations have been carried out using both model and full scale testing.

The steady state case, where the wing and infinite vortex are at zero relative velocity, has been solved for three-dimensional wings. A lifting line theory is used by Jones and Rao[9] and only slight im improvements have been made using a lifting surface theory shown by Kfoury[11].

The unsteady case, where the wing passes through a near the vortex has not yet been completely solved for the three-dimensional case. Johnson[7,8] uses a lifting surface theory on an infinite aspect ratio wing and has found the simplified lifting line approach inadequate. His paper calculates the peak to peak section lift coefficients obtained as a blade cuts through a vortex and compares them to the experimental study of Surendraiah[17]. Although the lifting surface theory does not always agree with the experiment, it is consistently much better than a lifting line approximation.

Surendraiah's experimental model consists of a single bladed rotor, 2 inches in chord and 12 inches in span, fitted with four chordwise pressure sensors located at a spanwise station of 95 per cent

of the rotor's radius. The rotor was operated at a high advance ratio in the proximity of a tip vortex generated by a fixed wing upstream. The rotor was rigidly mounted at a zero collective pitch without flapping or lagging. Data was taken for rotor plane positions above and below the vortex axis and for different intersection angles. Two values of rotor RPM and vortex strengths were used.

III. DEVELOPMENT OF THE UNSTEADY COMPUTATIONAL MODEL

Considerations from Thin Airfoil Theory

The potential flow about an airfoil can be calculated using two-dimensional thin airfoil theory to determine the pressure distribution and forces acting on the airfoil. The flow must satisfy the condition that the velocity normal to the airfoil surface be zero. In the classical solution a continuous distribution of vortices is placed on the camber line. Their strengths are then adjusted to induce velocities which , when added to the free stream velocity, give resultant velocities tangent to the camber line. If the strength of the vortex sheet is γ per unit length, an element of strength γdx placed at x will induce a velocity perpendicular to the airfoil at point ξ (for small camber as:

$$dv = \gamma dx/2\pi(x-\xi) \ . \tag{1}$$

The total velocity induced at ξ by the distribution of vorticity is given by the integral:

$$v = 1/2\pi \int_{o}^{c} (\gamma(x)dx/(x-\xi))dx \ . \tag{2}$$

The induced velocity at ξ must equal the component of the free stream normal to the chord at this point to insure no flow through the airfoil. If z is the vertical displacement of the mean camber line from the chordline, the relation is:

$$1/2\pi \int_0^c (\gamma(x)dx/(x-\xi))dx = -V(\alpha-(dz/dx)_\xi) \quad . \tag{3}$$

A γ distribution may now be specified given an airfoil geometry and angle of attack. Some restriction must be placed on the choice of a γ distribution to insure the flow will leave the trailing edge smoothly as observed experimentally. Any nonzero γ at the trailing edge will give an infinite velocity and therefore γ is restricted to zero to satisify the Kutta condition.

$$\gamma(c) = 0$$

It is shown in a number of aerodynamics texts, as Reference 4, that the γ distribution which satisfies both the tangency and Kutta boundary conditions is given by:

$$\gamma(x) = 2V[Ao(1 + \cos\theta/\sin\theta) + \sum_{n=1}^{\infty} An \sin n\theta] \qquad (4)$$

where

$$Ao = \alpha - 1/\pi \int_{o}^{\pi} dz/dx \, d\theta$$

$$An = 2/\pi \int_{o}^{\pi} dz/dx \cos n\theta \, d\theta$$

$$\theta = \cos^{-1} (1 - 2x/c)$$

Since the γ distribution is known (given the airfoil geometry and angle of attack), the lift and moment can be computed by considering the velocity just above and below a vortex sheet. The circulation around a differential element of a vortex sheet is:

$$2 \Delta V \, dx = \gamma dx \qquad (5)$$

A Bernoulli equation is now written between the upper and lower surfaces. If the pressure at a distance for from the airfoil is p_∞,

$$1/2\ \rho\ V^2 + p_\infty = 1/2\ \rho\ (V+\Delta V)^2 + p_u + \rho\ \partial\phi_u/\partial t \qquad (6)$$

and

$$1/2\ \rho\ V^2 + p_\infty = 1/2\ \rho\ (V-\Delta V)^2 + p_\ell + \rho\ \partial\phi_\ell/\partial t \qquad (7)$$

The difference in pressure across the airfoil is given by:

$$\Delta p = \rho V\gamma + \rho\partial/\partial t\ (\phi_u - \phi_\ell)$$

The lift per unit span is the integral of the chordwire pressure difference.

$$\ell = \int_0^c \Delta p dx$$

or

$$\ell = \rho V\Gamma + \rho \int_0^c \partial/\partial t \ (\phi_u - \phi_\ell) dx \qquad (8)$$

The second term represents the lift due to unsteady pressures and is equal to zero for the st dy state problem. Nondimensionalizing by the free stream dynamic pressure and chord, the section lift coefficient becomes:

$$C_\ell = 2/Vc \int_0^c \gamma dx \qquad (9)$$

When the expression for γ is reduced to the case of a flat plate airfoil, the C_ℓ is given by:

$$C_\ell = 2\pi\alpha \ .$$

The moment coefficient is written about the axis of rotation, a, as shown in Figure 1. It is noted that the axis position is in terms of semi-chord lengths, b, and is positive downstream of the mid-chord.

The distance from the axis to a vortex position x is given by $b(1 + a) - x$. The moment coefficient, where nose up is positive, is:

$$C_m = -2/Vc^2 \int_o^c (b(1+a)-x)\ \gamma dx \ . \qquad (10)$$

For the flat plate airfoil, the expression reduces to:

$$C_m = \pi/2\ (1+2a)\alpha$$

Steady State Computational Model

The computational model is based on the premise that a discrete number of point vortices placed on the mean camber line of a thin airfoil can approximate a continuous distribution. Figure 2 shows the geometrical arrangement of the vortices for the case of three control points. A control point is defined as a position where the velocity components are added to satisfy the flow tangency boundary condition. It is noted that the chord length is divided into equal length panels with a vortex and control point located at the 1/4 and

3/4 panel length positions respectively. The placement of the vortices is an extension of the Weissinger lifting line approximation and has proved to give satisfactory results in both steady and unsteady calculations. The Kutta condition is met automatically using this model due to the fact that the last control point is placed downstream of the last vortex. This placement allows the last vortex to have whatever strength required to give smooth flow from the trailing edge. When shed vortices are introduced for the unsteady problem, the last vortex may have a strength much greater than zero due to the induced velocities from the shed vortices. In the limit as Δx approaches the differential quantity dx, the statement of the Kutta condition, $\gamma(c) = 0$, will be met.

James[6] has shown conclusively that the choice of 1/4 and 3/4 points is both optimum and mandatory for the solution of any vorticity distribution in the steady two-dimensional problem. Exact lift and moment values are obtained regardless of the number of vortices placed on the airfoil. The value of γ_i at the first point vortex location is computed 12.4 per cent below the continuous value near the leading edge singularity for the flat plate airfoil. The γ_i values computed downstream of the first have negligible error.

The previous equations, in terms of a continuous $\gamma(x)$, are now

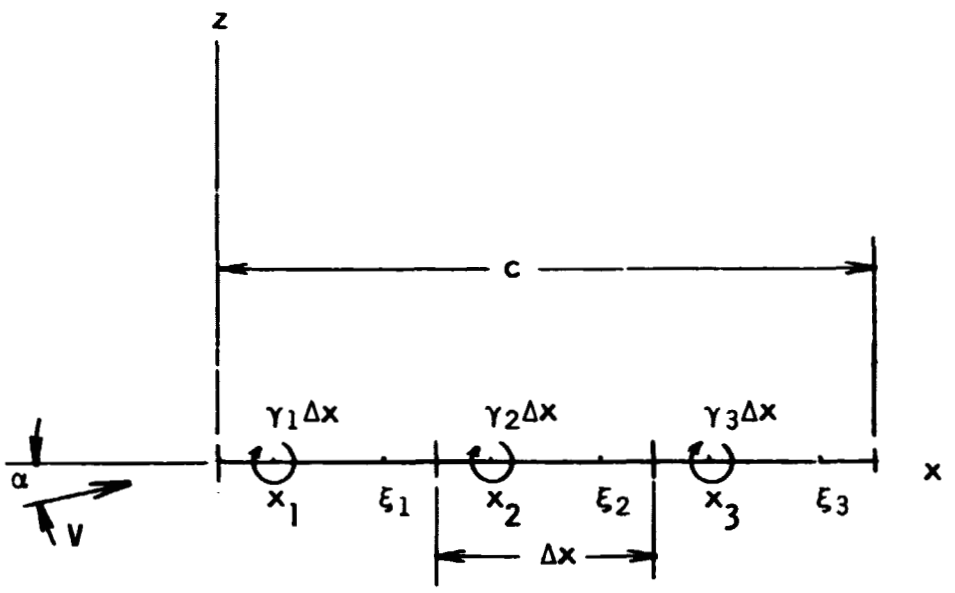

Figure 2 Three vortex computational Model

written in a finite difference form. Equation 3 at a control point ξ_j for n bound vortices becomes:

$$1/2\pi \sum_{i=1}^{n} \gamma_i \Delta x/(x_i-\xi_j) = - V(\alpha - (\Delta z/\Delta x)_j) \qquad (11)$$

The above expression leads to a matrix formulation of the problem of order n when all n control points are considered. For the example case of three vortices, the equations in matrix form are:

$$\begin{bmatrix} A_{11} & A_{12} & A_{13} \\ A_{21} & A_{22} & A_{23} \\ A_{31} & A_{32} & A_{33} \end{bmatrix} \begin{bmatrix} \gamma_1 \Delta x \\ \gamma_2 \Delta x \\ \gamma_3 \Delta x \end{bmatrix} = \begin{bmatrix} B_1 \\ B_2 \\ B_3 \end{bmatrix}$$

The coefficient matrix, A_{ij}, represents constant values determined from the geometry. The constants B_j represent the normal component of the free stream velocity at the control point.

A matrix of this form is solved by conventional means since it is square, linear, nonsingular and has constant coefficients. The method chosen to solve the matrix is the Banachiewicz - Crout algorithm which is essentially a process of successive elimination of unknowns by algebraic manipulation. The method has been programmed by Degelman[2] and used as a subroutine of the main program shown in the appendix.

With the values of the vortex strengths known, the lift and moment coefficients are computed using the finite difference form of equations 9 and 10.

$$C_{\ell} = 2/Vc \sum_{i=1}^{n} \gamma_i \Delta x \tag{12}$$

$$C_{m} = -2/Vc^{2} \sum_{i=1}^{n} (b(1+a)-x_i)\gamma_i \Delta x \tag{13}$$

Figure 3 shows the γ distribution on a flat plate airfoil obtained using a 3 and 6 vortex model. The γ_i values at the downstream stations are nearly exact while the first is about 12 percent low. The accuracy of the lift and moment calculations is exact for both cases which confirms the results of James[6]. Note that the γ_i values have been converted to an equivalent distributed value to compare with equation 4.

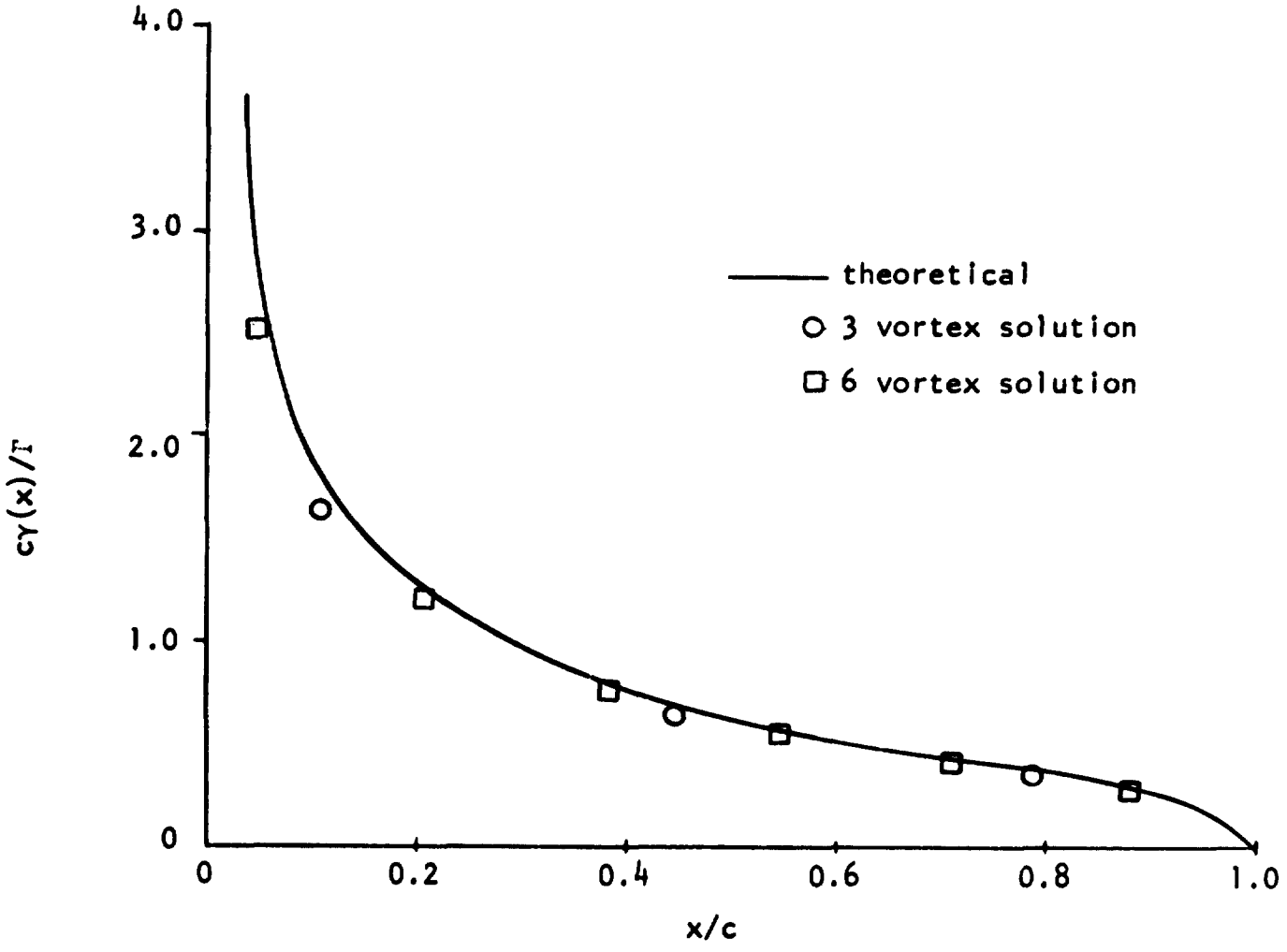

Figure 3 Steady State Gamma Distribution

Unsteady Flow Considerations

The physical principle which is of primary importance to unsteady problems is the conservation of circulation. The time rate of change of bound circulation and the wake circulation must be zero.

$$d\Gamma/dt = d\Gamma b/dt + d\Gamma w/dt = 0 \qquad (14)$$

Equation 14 is a result of Kelvins' theorem and states that the net circulation around both the airfoil and wake must remain a constant. Thus if the bound circulation changes due to flow fluctuations or airfoil motion, there must be an equal but opposite change in the wake. The circulation change in the wake is known to take place at the trailing edge in the form of shed vortices.

The vortex sheding procedure in two dimensions is shown in Figure 4. At time t_1 there is no circulation on the airfoil or in the wake and at time t_2 the airfoil increases its angle of attack and sheds a starting vortex equal to the strength of the bound vorticity at that time. The shed vortex is formed at the trailing edge as Δt approaches zero for the continuous case and each new wake vortex has a strength equal to the change in bound circulation. The shed

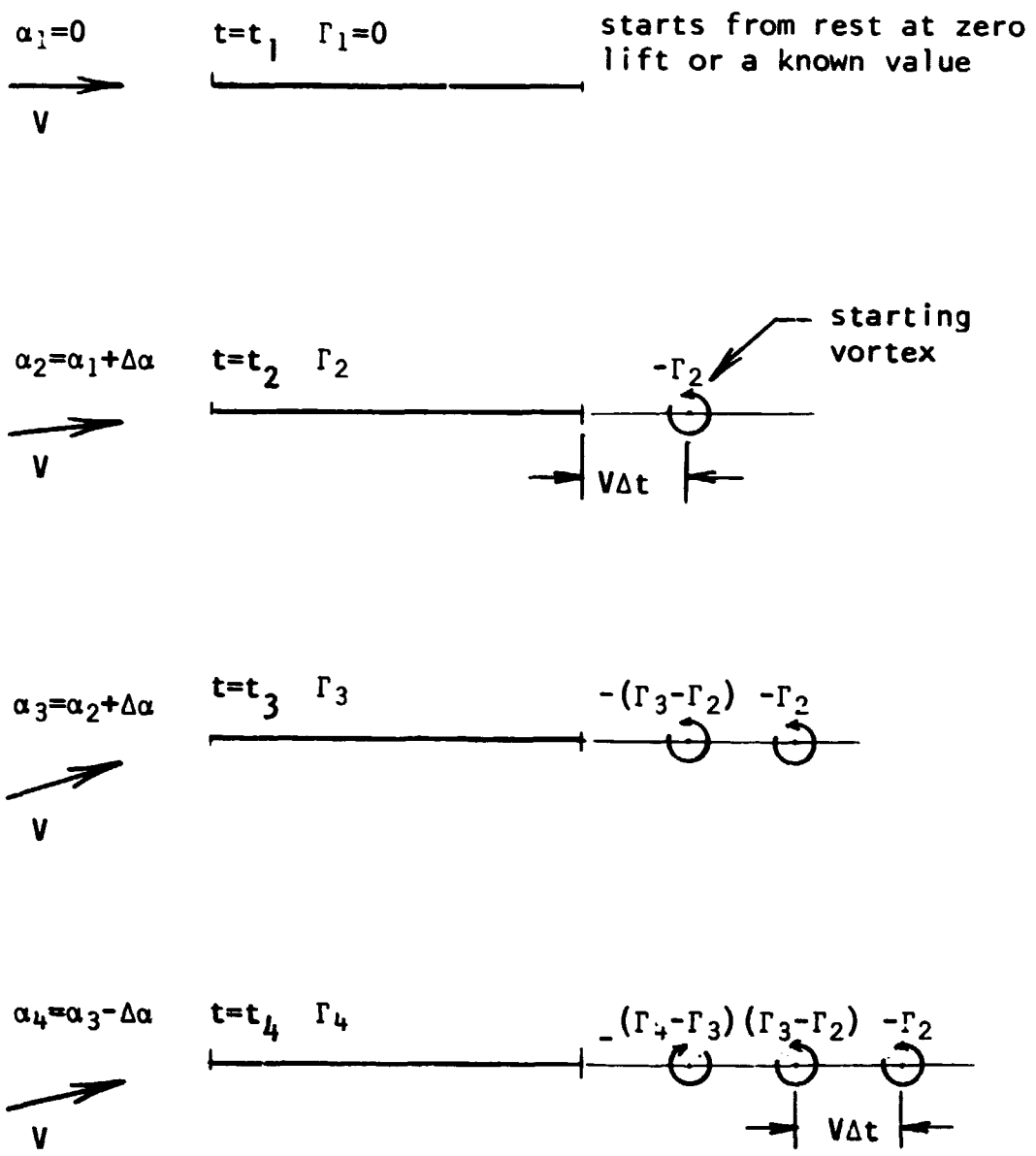

Figure 4 Unsteady Vortex Sheding

vortices move downstream with the free stream velocity and their path is influenced by the induced velocity of one element on another. The vortex sheding process continues until steady state conditions are reached, that is, the bound circulation does not change with time.

Computational Model Changes for the Unsteady Case

The difference in the equations forming the matrix in the unsteady problem is the influence of the shed vortices on the velocity induced at a control point. At time t_2, as shown in Figure 4, the velocity at a control point due to the bound vortices at t_2, $\gamma^{(2)}$, the first shed vortex, $-\Gamma_2$, and the free stream is:

$$1/2\pi \sum_{i=1}^{n} \gamma_i^{(2)} \Delta x/(x_i-\xi_j) - 1/2\pi \sum_{i=1}^{n} \gamma_i^{(2)} \Delta x/(c-\xi_j+V\Delta t) = - V(\alpha + (\Delta z/\Delta x)_j) \tag{15}$$

Writing equation 15 for all n control points and solving the matrix

for $\gamma_i^{(2)}$, the value of Γ_2 is computed as:

$$\Gamma_2 = \sum_{i=1}^{n} \gamma_i^{(2)} \Delta x$$

During the time interval t_2 to t_3 another shed vortex is formed of strength $-(\Gamma_3 - \Gamma_2)$. The first shed vortex continues to move downstream to a position $2V\Delta t$ from the trailing edge. The velocity at a control point influenced by two shed vortices at time t_3 is:

$$1/2\pi \sum_{i=1}^{n} \gamma_i^{(3)} \Delta x/(x_i - \xi_j) - 1/2\pi \left[\sum_{i=1}^{n} \gamma_i^{(3)} \Delta x - \Gamma_2 \right]/(c - \xi_j + V\Delta t)$$

$$- 1/2\pi \, \Gamma_2/(c - \xi_j + 2V\Delta t) = - V(\alpha + (\Delta z/\Delta x)_j)$$

As time proceeds, the prccess adds another shed vortex at each time increment. A general form for a time interval m is:

$$1/2\pi \sum_{i=1}^{n} \gamma_i^{(m)} \Delta x/(x_i-\xi_j) - 1/2\pi[\sum_{i=1}^{n} \gamma_i^{(m)} \Delta x - \Gamma(m-1)]/(c-\xi_j+V\Delta t)$$

$$1/2\pi \sum_{k=1}^{(m-1)} (\Gamma_k - \Gamma(k-1))/(C-\xi_j+(k+1)V\Delta t) = -V(\alpha+(\Delta z/\Delta x)_j) \qquad (16)$$

It is noted that the unknown γ distribution appears both in the expression for the bound and new shed vortices' influence on the control point. This property of the unsteady problem changes the form of the coefficient matrix used in the calculations.

The lift and moment can be computed using the unsteady Bernoulli equation. The unsteady part of the equation makes a contribution to the lift (from equation 8) as:

$$\rho \int_0^c \partial/\partial t \, (\phi_u - \phi_\ell) \, dx \quad .$$

A velocity pctential is written from the leading edge to a position x on the airfoil for the upper and lower surfaces.

$$\phi_u = \int_0^x (V + \Delta V) \, dx$$

$$\phi_{\ell} = \int_{o}^{x} (V-\Delta V)\, dx$$

Then

$$\phi_u - \phi_{\ell} = \int_{o}^{x} 2\Delta V\, dx$$

and from equation 5

$$\phi_u - \phi_{\ell} = \int_{o}^{x} \gamma\, dx \tag{17}$$

The total lift in terms of the γ distribution on the airfoil is:

$$\ell = \rho V \int_{o}^{c} \gamma\, dx + \rho \int_{o}^{c} [\partial/\partial t \int_{o}^{x} \gamma\, dx]\, dx \tag{18}$$

The unsteady lift is composed of two parts, one independent of time and the other due to the time rate of change of circulation around

the airfoil. Although part of the lift appears to be independent of time, it is not the same lift that would be computed using steady state methods. The γ distribution is altered by the wake, and the time history of the unsteady motion must be known to compute the wake structure. The second term of equation 18 is not to be confused with the term "added" or "apparent mass" used in the classical theories[10, 14, 18]. Apparent masses are characteristically independent of the past history of the motion and are noncirculatory in nature.

Airfoil motion may be defined as angular rotation about some axis on or off the airfoil and vertical translation of the axis. Either motion induces velocity components normal to the airfoil and must be included in the sum of velocities at each control point. A positive rotation (nose up) effects each control point as:

$$v_{\alpha} = d\alpha/dt \, [b(1 + a) - \xi_j]$$

A positive vertical motion effects all control points as:

$$v = - dh/dt$$

The direct integration of the unsteady Bernoulli equation provides a convenient means of finding the forces on an airfoil in a numerical procedure. Problems of airfoil motion or flow unsteadiness can be handled since the bound vortex distribution and wake structure is generated at each time increment for any inflow condition. Airfoil motion or gust structure is not limited to any particular type.

Discussion of the Wake Geometry

The preceding unsteady model assumes the shed vortices lie in the x direction and move downstream with the flow velocity. In reality the wake rolls up under its own influence and the influence of the bound vortices. Djojodihardjo and Widnall[3] have shown the effects of using three different wake geometries for the impulsively started airfoil problem. With the lift build up produced by a free wake (or field-induced wake) as the standard, the rigid wake assumption gives essentially no error for small angles of attack. Even at 0.3 radians the difference is less than 4% for the first 1.25 semi-chord lengths after starting. As the distance traveled increases the results for the free and rigid wake approach each other. No significant difference is noted between a rigid wake which lies in the x direction or one

which is aligned with the velocity vector. Giesing[5] compares a deforming wake result to the Wagner function for the step change in angle of attack problem and also shows the free wake to slightly retard the lift build up.

Giesing[5] has also compared the nonlinear results to two other classical problems which are the Kussner function used to find the lift on a flat plate entering sharp edge gust and the Theodorsen function used to find the lift on a flat plate executing periodic motions of small amplitude. The Kussner function was found to be unaffected by the nonlinearity even for the case where the vertical gust velocity is half that of the free stream. The Theodorsen function, however, is affected by the deforming wake by an amount proportional to the amplitude of the motion and its reduced frequency, k.

$$k = \omega b/V$$

The deviations from the linear theory increase with increasing amplitude and reduced frequency. For vertical oscillations with an amplitude of 0.06 C, the nonlinear effects are noticeable above a k of 1.0. The lift is always nearly in place but the magnitude is above that

calculated by linear methods. At an amplitude of 0.3 C, the circulatory lift is twice that predicted by Theodorsen at a k of 1.0. The noncirculatory effects are important at large amplitudes and high frequencies, however, and should be considered when comparing the total lift obtained from linear and nonlinear methods. These effects are proportional to k^2 and can completely dominate the lift at high reduced frequencies.

IV. COMPARISON OF UNSTEADY COMPUTATIONS TO THEORY

Before applying the unsteady numerical solution to the airfoil-vortex interaction problem, its validity was assessed by comparing it to the Theodorsen function for an oscillating airfoil and the Wagner function for the impulsive start problem. A comparison with the Theodorsen function provides a check on both circulatory and "added mass" parts of the lift and the Wagner function comparison is of importance since a numerical method requires small step changes in the inflow to proceed from one time step to the next. A satisfactory comparison with both Theodorsen and Wagner functions will give confidence in the results obtained for any other problem.

Theodorsen Function Comparison

The problem of an airfoil oscillating in the vertical and rotational coordinates is considered. The theoretical expression of the lift for this case is written:

$$\ell = 2\pi \rho V C(k)[\dot{h}' + V\alpha + b(1/2-a)\dot{\alpha}] + \pi \rho b^2 [\ddot{h}' + V\dot{\alpha} - ba\ddot{\alpha}] \tag{19}$$

Where C(k) is the Theodorsen function made up of real and imaginary parts as:

$$C(k) = F(k) + i\,G(k)$$

Equation 19 is derived for harmonic motion where the vertical coordinate h' and the rotation angle α are written:

$$h' = h_o' e^{i\omega t} \tag{20}$$

$$\alpha = \alpha_o e^{i\omega t} \tag{21}$$

Substituting the above and their time derivatives into equation 19, separating the real and imaginary parts and normalizing by $\rho V^2 b$. The following expression is obtained for the $C\ell$:

$$C_\ell = \bar{A} e^{i(\omega t+\phi)} \tag{22}$$

where

$$\overline{A} = (BB^2 + CC^2)^{1/2}$$

$$\phi = TAN^{-1}(CC/BB)$$

and

$$BB = \pi [\alpha_o (k^2 a + 2F - 2Gk(1/2-a)) - h_o' (k^2/b + 2Gk/b)]$$

$$CC = \pi [\alpha_o (k + 2F (1/2 - a) k + 2G) + h_o' (2Fk/b)]$$

$\overline{A}$ is the amplitude of the lift predicted by Theodorsen and ϕ is the phase angle. To compare this result to the lift calculated by steady state methods, consider the C_ℓ obtained using only the instantaneous vertical velocity and angle of attack:

$$C_\ell ss = 2\pi(\alpha + \dot{h}'/V)$$

Again using equations 20 and 21 and their time derivatives, an expression for the steady state lift coefficient can be written.

$$C_{\ell}ss = \bar{A}ss\ e^{i(\omega t+\beta)} \tag{23}$$

where

$$\bar{A}ss = 2\pi(\alpha_o^2 + (\omega h_o'/V)^2)^{1/2}$$

$$B = TAN^{-1}\ [(\omega h_o'/V)/\alpha_o]$$

The ratio of the actual C_{ℓ} to that computed with steady state methods becomes:

$$C_{\ell}/C_{\ell}ss = \bar{A}/\bar{A}ss\ e^{i(\phi-\beta)}$$

For illustration the ratio of $C_{\ell}/C_{\ell}ss$ and the phase difference $(\phi-\beta)$ are plotted as a function of reduced frequency on Figure 5 for vertical oscillations and Figure 6 for rotational oscillations. The

theoretical magnitude ratio and phase difference are shown as solid lines and the data points are values obtained by the numerical computations.

The computations were made using six bound vortices to represent the γ distribution. This was found to be a satisfactory number for the reduced frequencies tested. Increasing the number improves the results only slightly at high k values.

Typical results from the numerical computations are shown on Figure 7. The ratio of C_ℓ to maximum $C_\ell$ss is plotted against ωt for k's of 0.2 and 10. Values obtained using the computational model are in agreement with Theodorsen's results both for a k of 0.2 where wake effects cause the greatest phase lag and for a k of 10 where the non-circulatory effects are significant. The computed C_ℓ value occuring at the second peak is 4.5 per cent above the exact for a k of 0.2 and 8.0 per cent above a k of 10. The errors generally increase with k and fall within the range of 0 per cent at a k of zero to 8 per cent at a k of 10.

The accuracy is a function of how small the time interval is between successive solutions. To obtain the accuracy quoted, it is necessary to make 60 solutions per cycle for an amplitude of 0.15 radians. The time increment, Δt, for 60 solutions per cycle is $\pi/30\omega$.

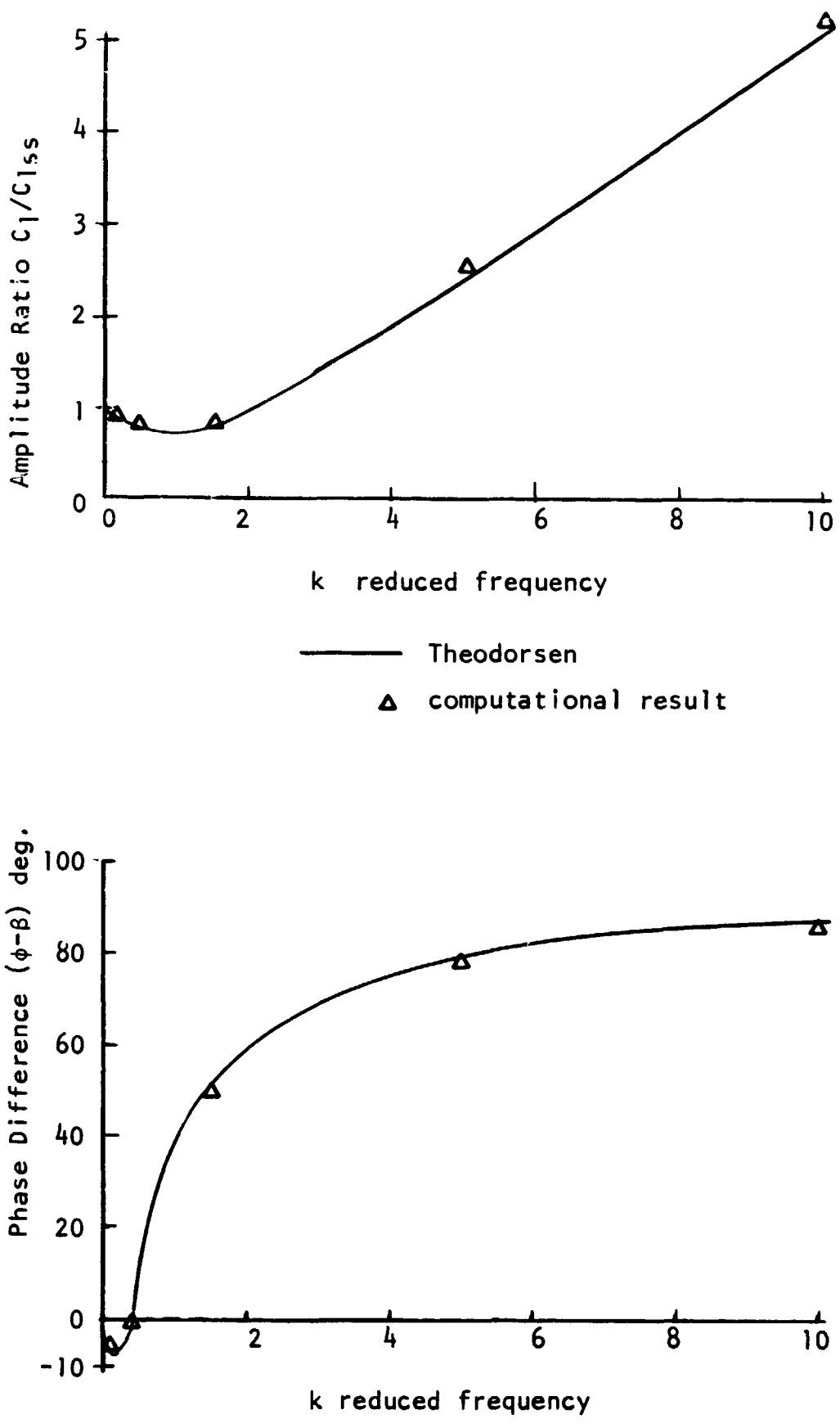

Figure 5 Accuracy of Numerical Solution for a Vertically Oscillating Airfoil

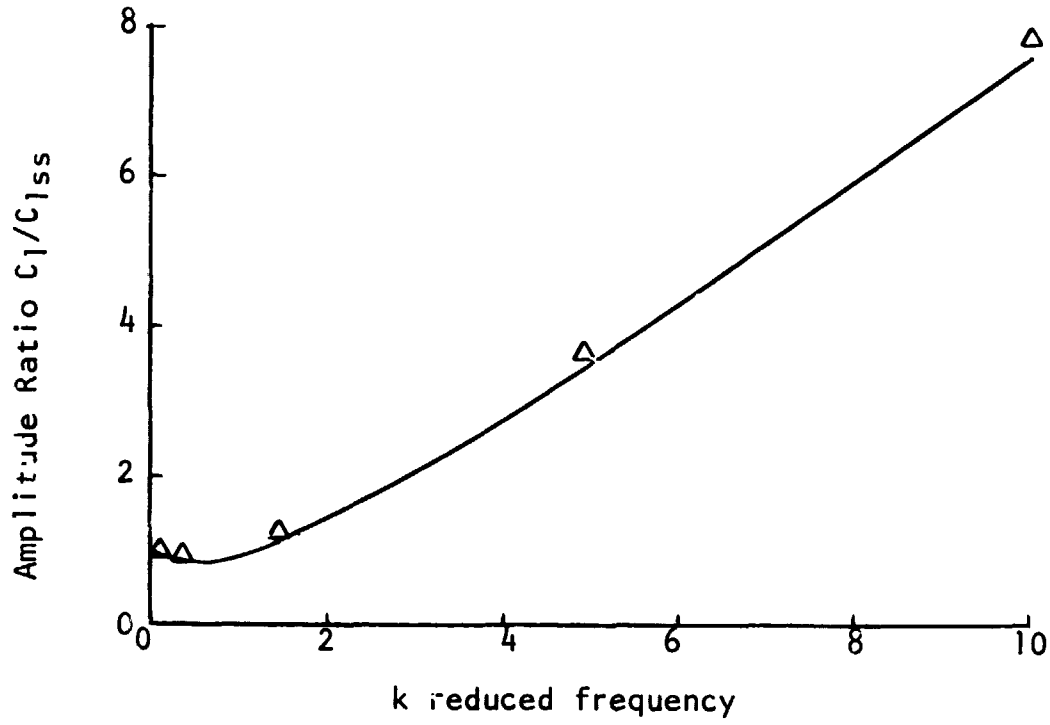

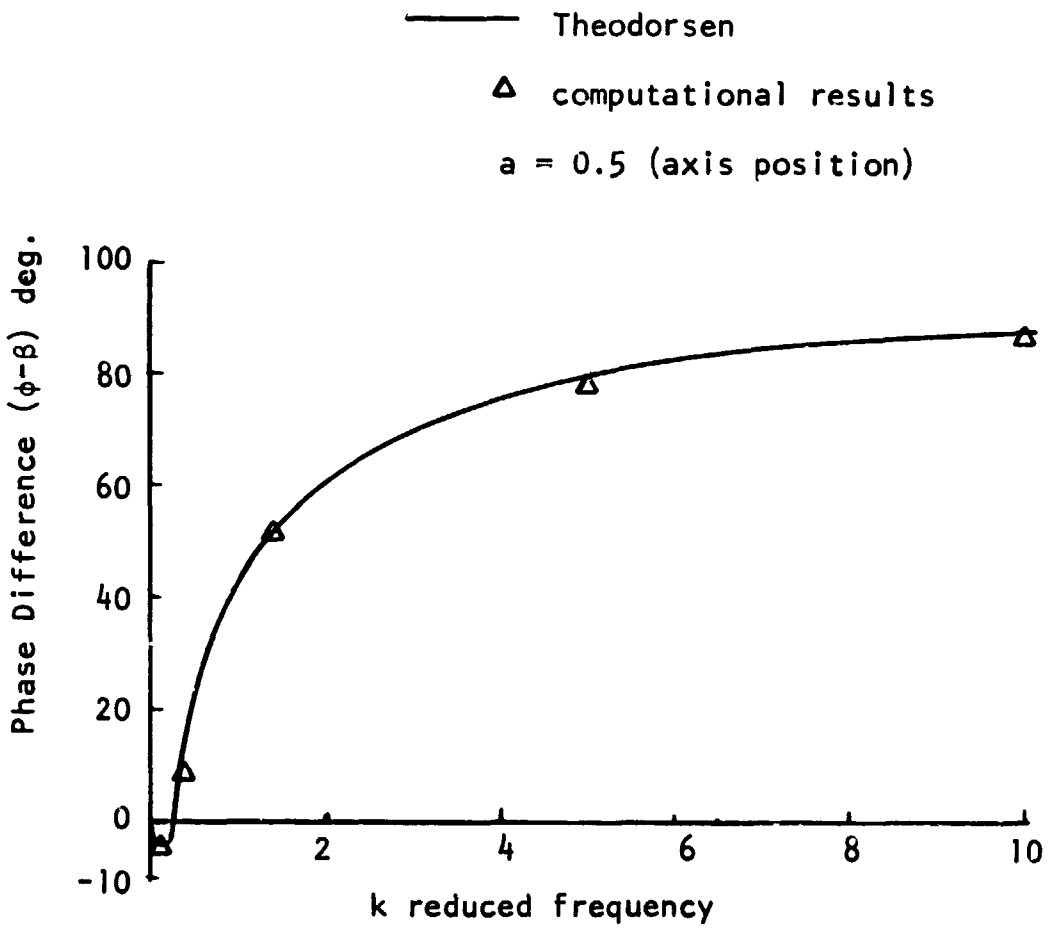

Figure 6 Accuracy of Numerical Solution for an Airfoil Oscillating in Rotation

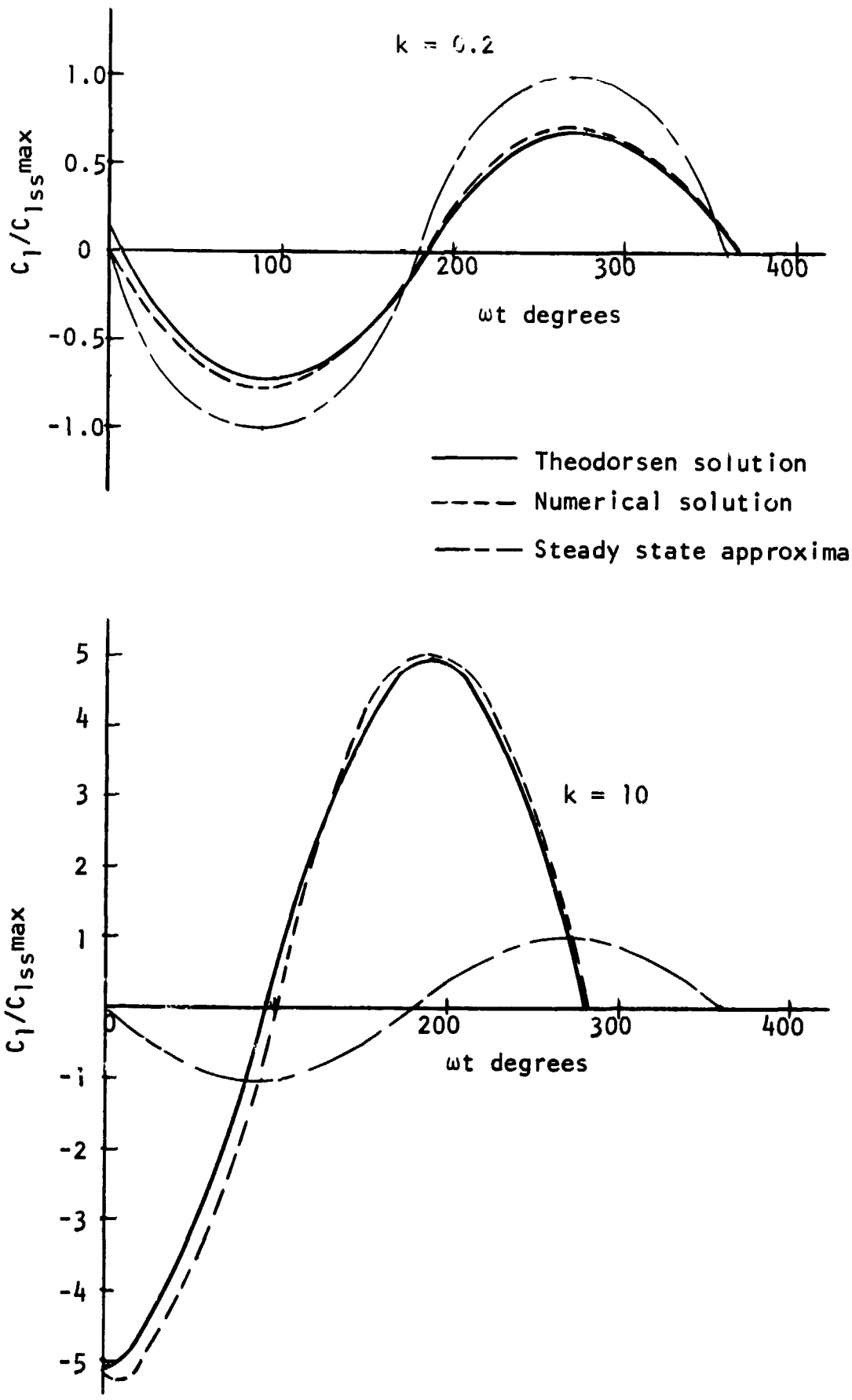

Figure 7 Typical Periodic C_1 for k = 0.2 and 10

It is of interest to note the difference in lift calculated using unsteady methods to that obtained assuming steady state as shown in Figure 7. The k of 0.2 gives a 27 per cent reduction in the amplitude and a phase lag of 7 degrees from the steady state calculation. The k of 10 gives a factor of 5 increase in the amplitude and phase lead of 84 degrees.

Wagner Function Comparison

The Wagner function gives the lift build up on an airfoil after an instantaneous change in the inflow conditions. A step change in the angle of attack, for example, causes the lift to change as a function of time as:

$$\Delta \ell = \pi c \rho V^2 \Delta\alpha \phi(s) . \tag{27}$$

The term $\phi(s)$ is the Wagner function in terms of s, the distance traveled in semi-chord lengths. The Wagner function is restricted to positive values of s and is written as[1]:

$$\phi(s) = 2/\pi \int_{k=o}^{\infty} F(k)/k \sin ks \, dk . \tag{28}$$

The integral ranges over all reduced frequencies to infinite values which indicates that the step change problem is considered a motion at an infinite frequency. The expression for $\phi(s)$ is not of simple form since F(k) is expressed in terms of Bessel functions, but a convenient approximation exists for $\phi(s)$ which is:

$$\phi(s) = s + 2/s + 4 \quad . \tag{29}$$

The circulatory part of the solution, that part which is time and wake dependent, is the only part included in the Wagner function and the contribution to the lift of the added mass must be included for the total lift to be obtained. It is only necessary to consider the non-circulatory contribution at the very start of the problem, however, since the inflow conditions change only at the start.

The comparison of the results from the computational model to the Wagner function is shown by Figure 8. It is clear that the accuracy of the computation depends directly on the time interval Δt chosen. This property is related to the fact that at the start of the problem, the inflow conditions change instantaneously causing a strong starting vortex to be shed which greatly effects the lift.

For this reason a detailed description of the wake is required at the start. It is clear that in the limit of a zero Δt, the computational procedure will give exactly the Wagner function except at the instant of starting where the lift would be momentarily infinite due to the added mass contribution.

The instantaneous γ distribution shortly after the start of the step change problem is shown in Figure 9. Notice that nearly as much negative as positive γ strength is present which indicates that most of the lift is resulting from the rate of change of circulation rather than the circulation itself. γ distributions of this general shape appear frequently in the unsteady calculations and it is clear that knowledge of the chordwise pressure distribution is necessary for accurate lift and moment computations.

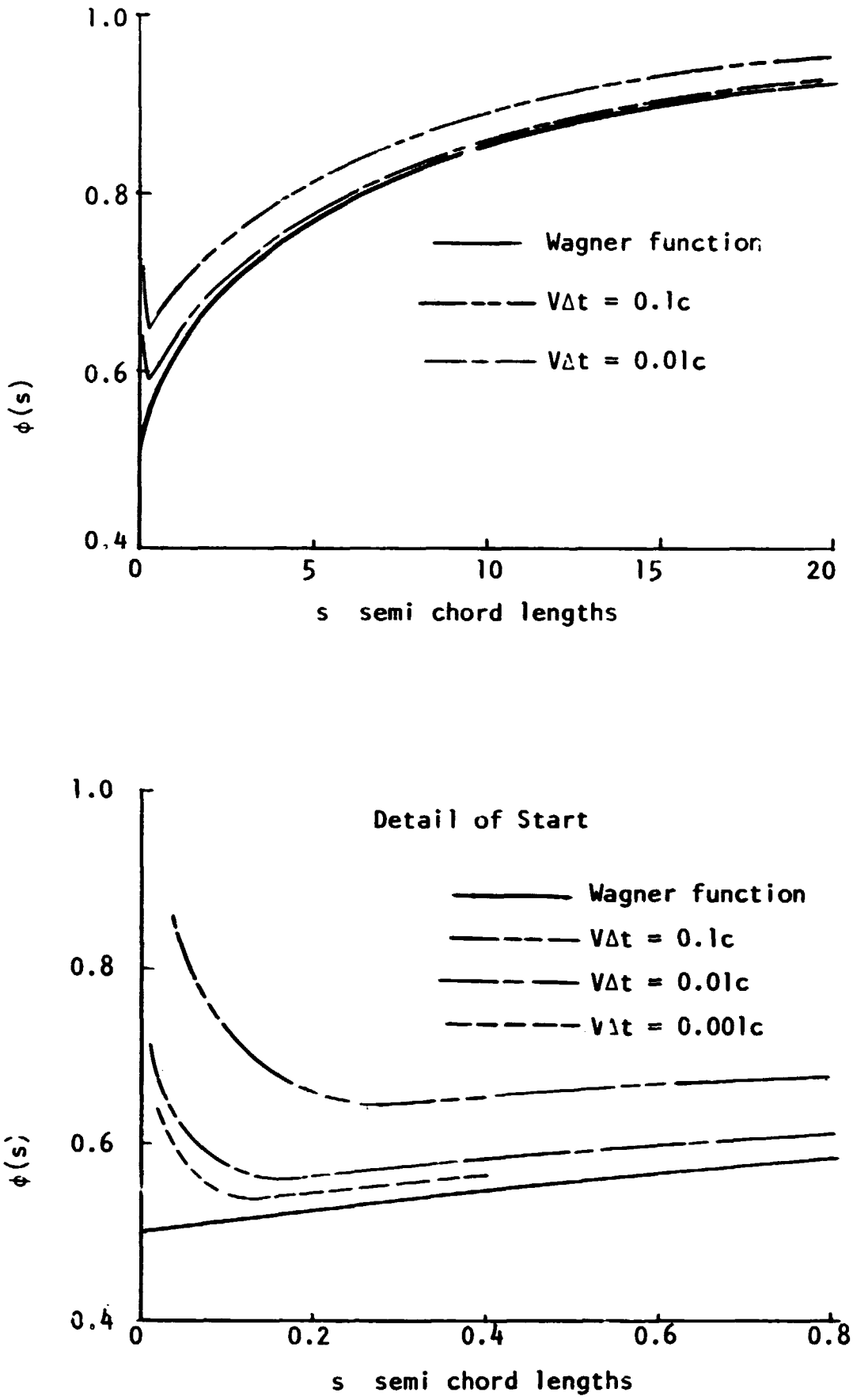

Figure 8 Comparison of Numerical Solution to Wagner Function

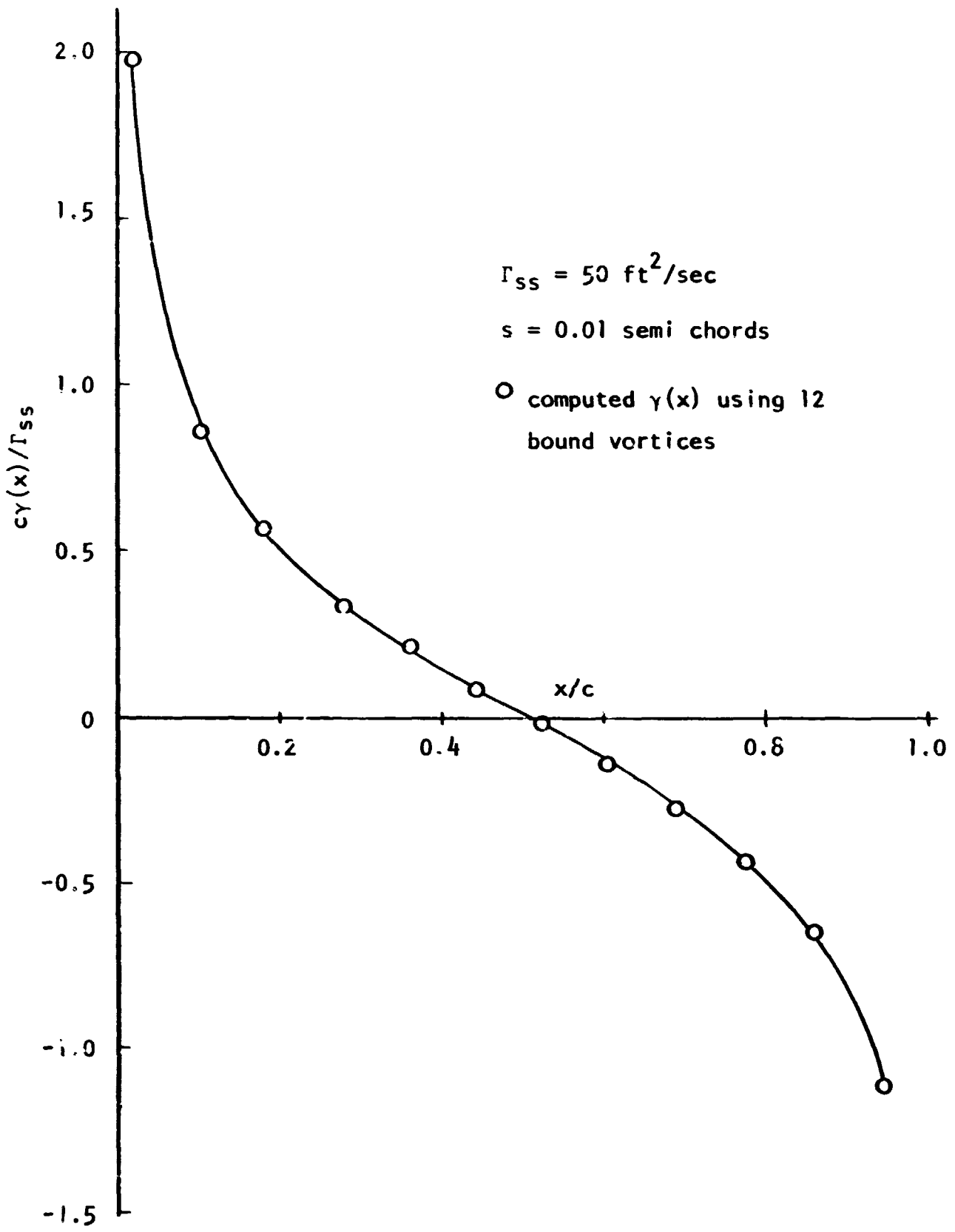

Figure 9 Chordwise γ distribution at start of Step Change Problem

V. APPLICATION OF THE COMPUTATIONAL MODEL TO THE ROTOR-VORTEX INTERACTION PROBLEM.

With confidence gained in the numerical method by comparison to the classical theories, the method was applied to the rotor-vortex interaction problem. The two-dimensional study was undertaken as an approximation to the case where the helicopter blade intersects a vortex whose axis passes parallel to the span as shown in Figure 10. The intersection angle for this case is 90 degrees. The entire blade enters the vortex at the same time and a two-dimensional loading is expected. For other intersection angles, fluctuations in both spanwise and chordwise loadings occur requiring an unsteady three-dimensional approach to the problem.

The vortex interaction model is basically the same as the unsteady airfoil problem with the addition of a potential vortex to the free stream. The vortex induces a different velocity at each control point which modifies the bound vortex strengths required to satisfy the boundary conditions. The vortex also effects the path of the wake vortices, but this effect is neglected since a rigid wake is assumed. In turn, the bound and wake vortices effect the path of the vortex due to their induced velocities at the vortex.

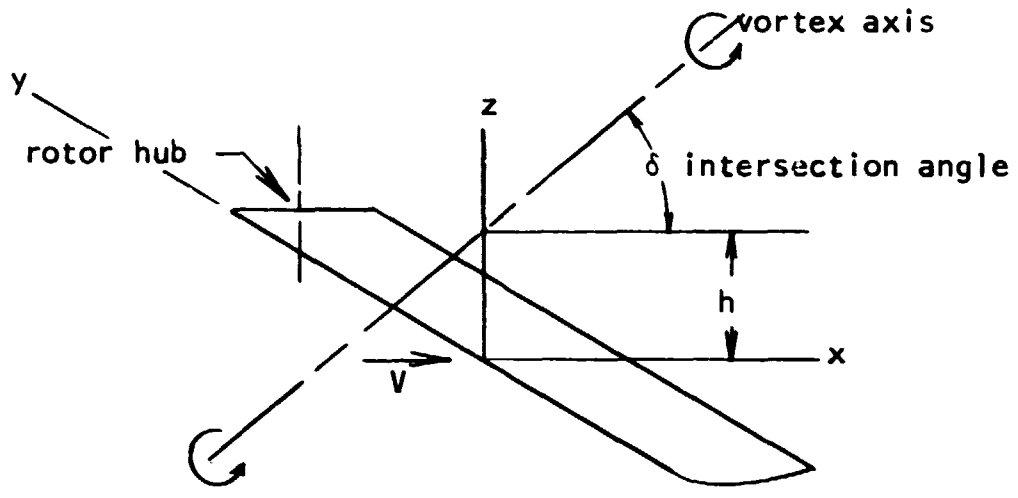

note: vortex axis in plane parallel to xy plane

vortex-induced angle of attack

vortex axis parallel to blade span - δ = 90 degrees

Figure 10 Blade-Vortex Intersection

In previous investigations of this problem, the vortex path has been assumed fixed, unaffected by the blade and wake. The consideration of the effect is found to be worthwhile when the blade passes near the vortex.

Including the vortex into the program involves the computation of normal and tangential velocity components induced at the control points. The normal component alters the bound vortex strengths and distribution required to maintain the boundary condition and the tangential component increases the effective velocity across the chord.

During the vortex interaction, the blade experiences a resultant velocity, V_r, which is in general different from that of the free stream due to the presence of the vortex. Since every control point experiences a slightly different horizontal component of the resultant velocity, V_x, the lift is computed from the following integral containing V_x.

$$\ell = \rho \int_0^c V_x \gamma(x)\, dx + \rho \int_0^c [\partial/\partial t \int_0^x \gamma(x)dx]dx \qquad (30)$$

The lift coefficient is based on the free stream velocity, however, as:

$$C_{\ell} = \ell/1/2\ \rho\ V^{2}\ c$$

From experience with periodic lift fluctuatic , it was found that a Δt which gives 60 solutions per cycle is required for reasonable accuracy. The Δt for the vortex interaction problem was determined by assuming the lift changes from a positive to a negative peak in about one chord length. Assuming this to be like a half-cycle, 30 solutions per chord length was used giving the following expression for Δt.

$$\Delta t = c/30\ V$$

The starting position of the vortex was chosen as 2 1/2 chord lengths ahead of the leading edge of the blade. While the furthest distance possible is desirable from a long wake generation standpoint, this value was found to be a practical limit when storage space and computation time requirements are considered. This has not been a severe limitation since the wake has proved to have its greatest effect when the vortex is near the blade.

VI. ANALYSIS OF RESULTS AND COMPARISON WITH EXPERIMENT

Important parameters for consideration in the blade-vortex interaction are shown on Figure 11. These include the initial height of the vortex above or below the blade, h, the blade chord length, the vortex strength, Γ_v, the positive and negative peak C_ℓ values and the time interval between them, ΔT, and the maximum difference of the section lift coefficient, ΔC_ℓ.

Typical computed C_ℓ variation and vortex path time histories are shown in Figures 11 to 14. The solutions correspond to Surendraiah's[17] experimental conditions of 2000 RPM and a Γ_v of 15.25 ft^2/sec. As the magnitude of h/c decreases, ΔC_ℓ increases, the first derivative of the C_ℓ curve changes more abruptly at the peak C_ℓ values, and the distance required to go from positive to negative peak C_ℓ values decreases from nearly two chord lengths at an h/c of 1.0 to less than one chord length at an h/c of 0.1.

Figure 14 presents a comparison of the computed C_ℓ variation through the vortex to a corresponding experimental trace where the value and position of the positve peak C_ℓ is matched to that computed. The general shape of the C_ℓ variation is similar although the

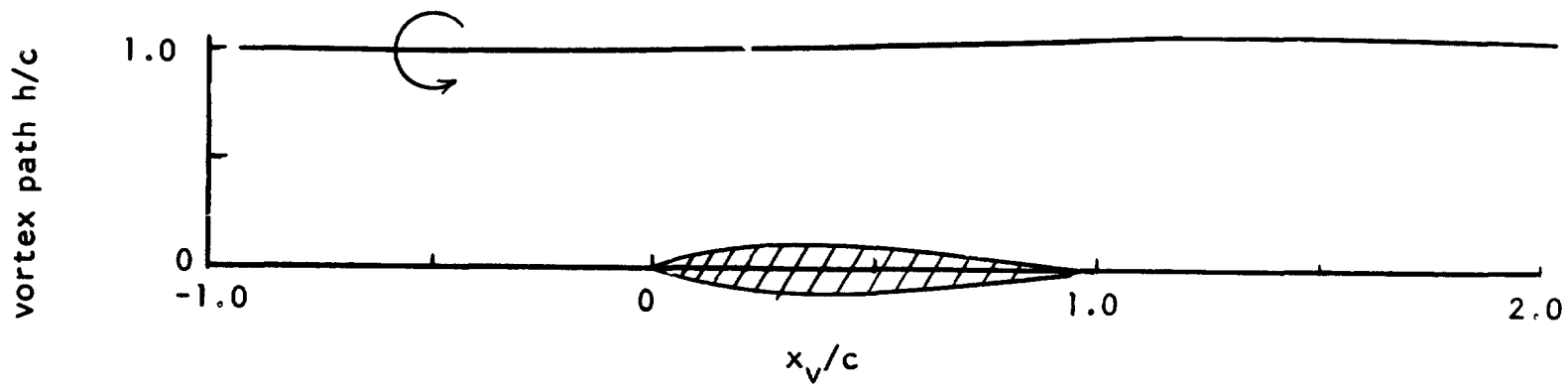

represents: h/c = 1.0 RPM = 2000 Γ_v = 15.25 ft^2/sec

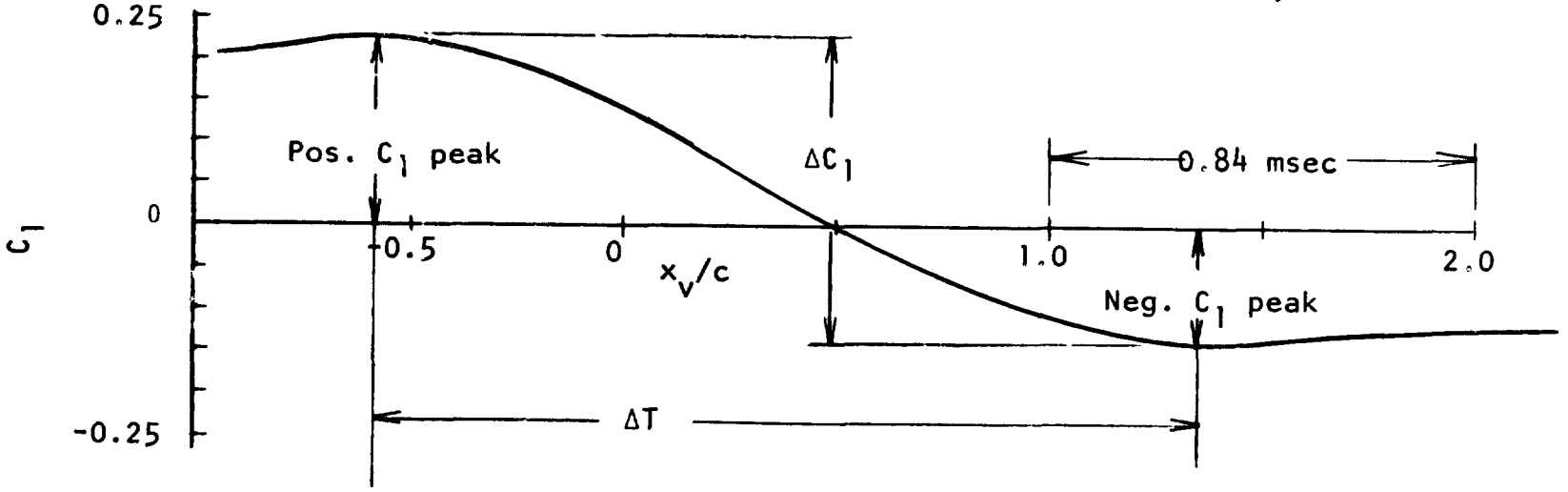

Figure 11 Computed C_l variation through Vortex for h/c = 1.0

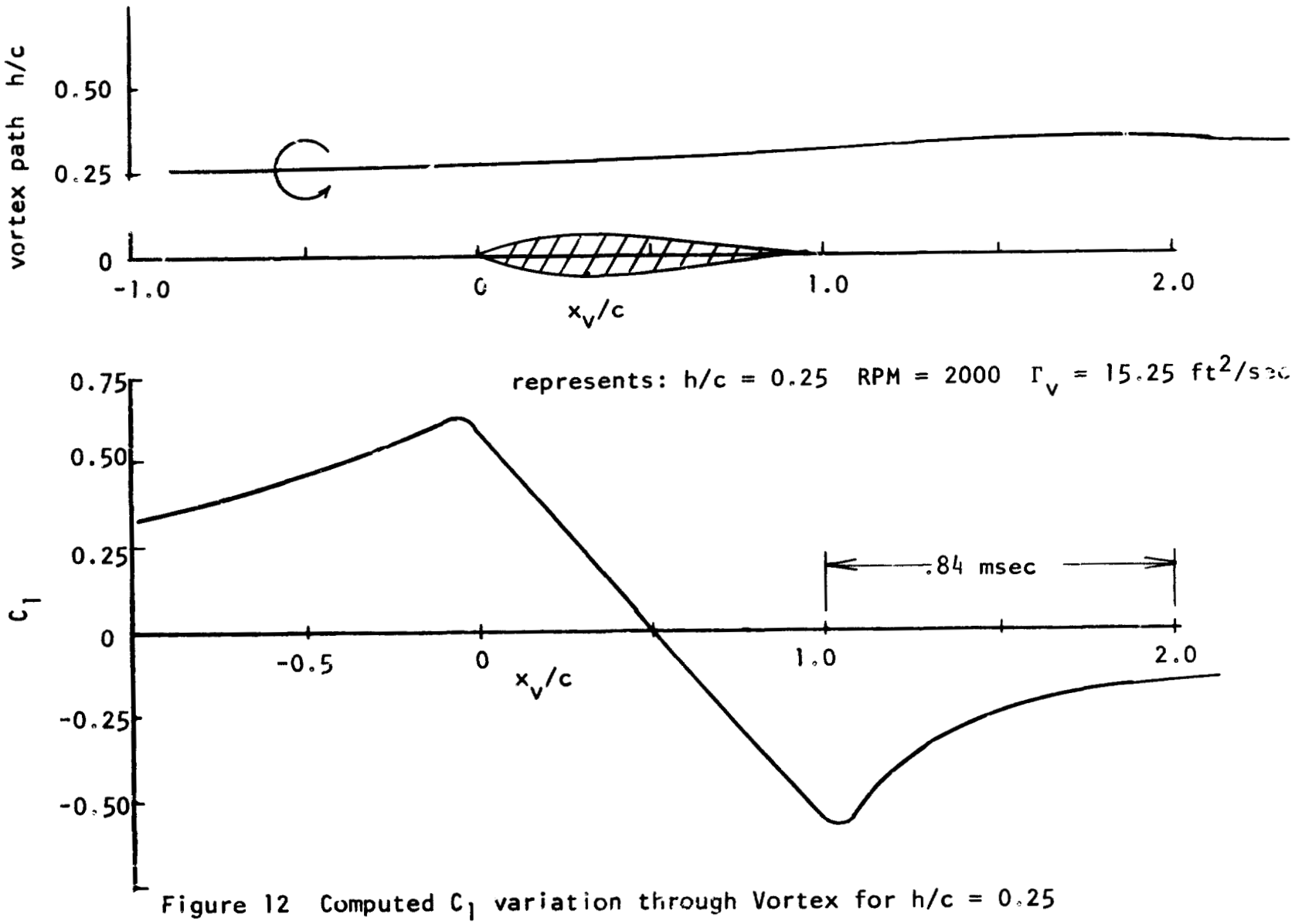

Figure 12 Computed C_l variation through Vortex for h/c = 0.25

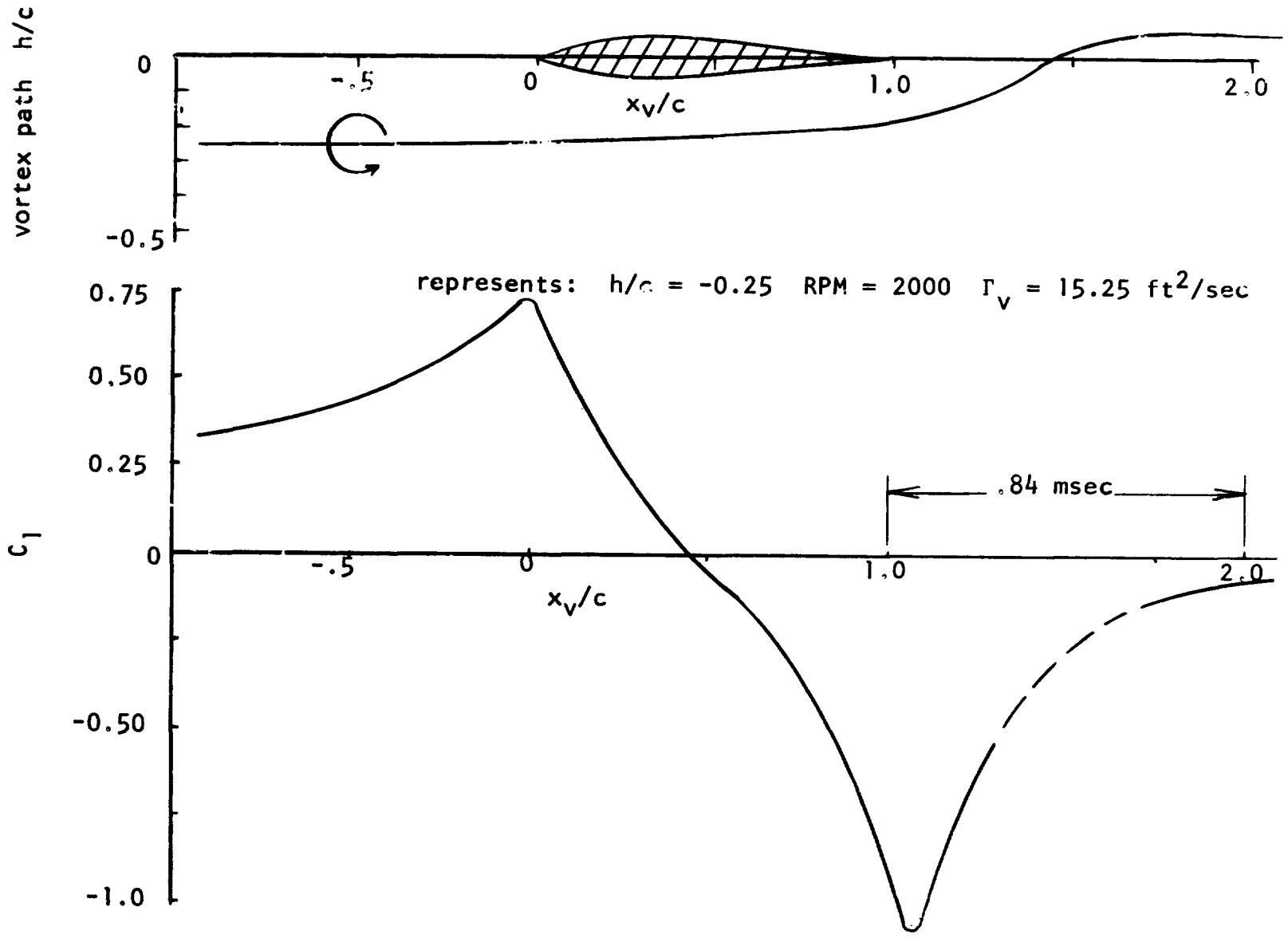

Figure 13 Computed C_l variation through Vortex for h/c = -0.25

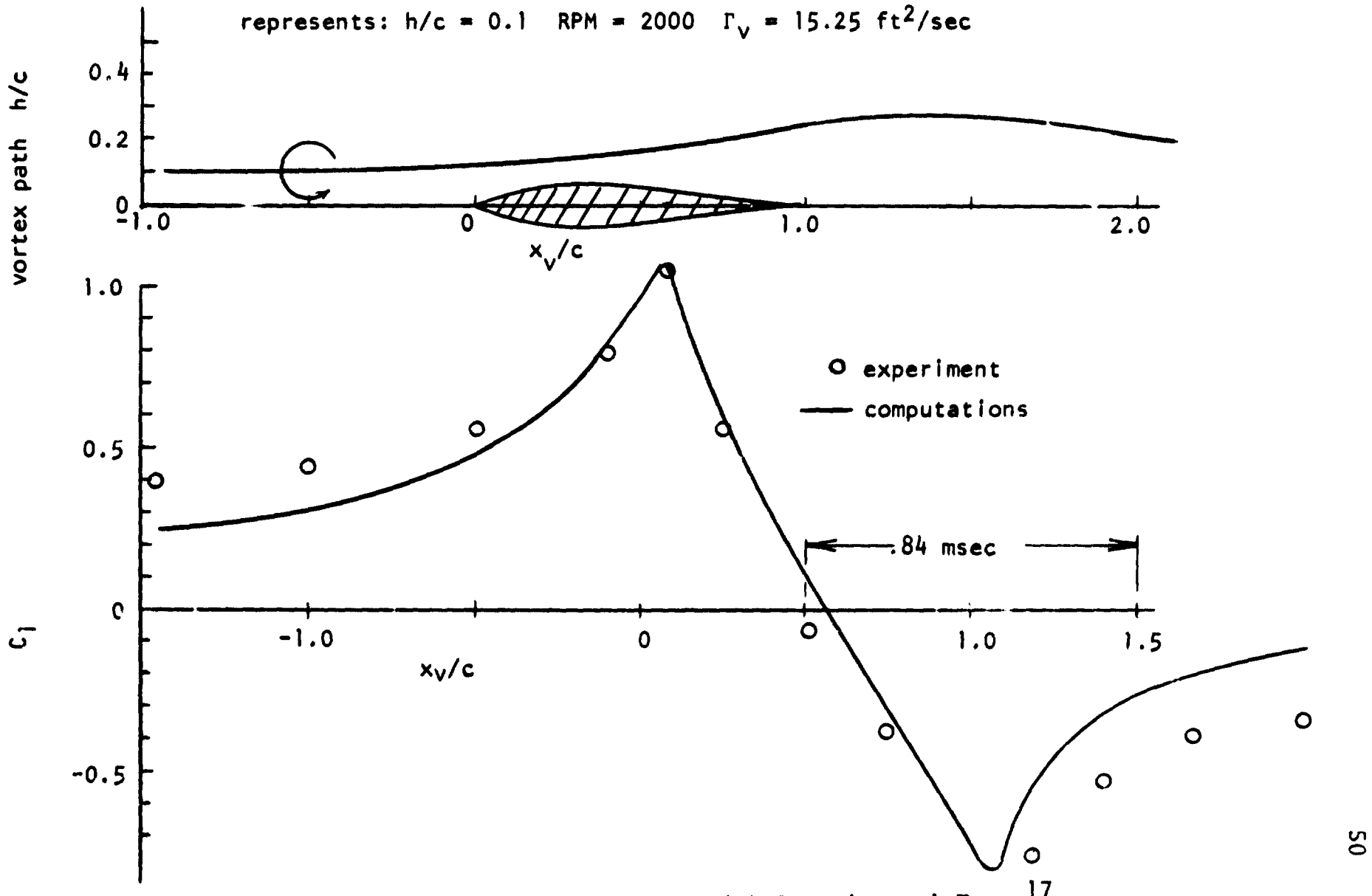

Figure 14 Computed C_l variation and Comparison with Experimental Trace[17]

computations predict a somewhat more rapid build up and decay of the lift.

Figure 15 shows the effect of using a quasi-steady approximation to compute the fluctuating lift on the blade. The lift is computed including the unsteady term in equation (30) but the wake's contribution to the lift is neglected. The positive and negative C_ℓ peak values, computed using the quasi-steady approximation, are well above those computed by unsteady theory. Including the wake in the calculations generally reduces the loads produced by the blade-vortex interaction.

A steady state approximation, computing the lift by the instantaneous velocity and angle of attack, is also shown by Figure 15. The peak C_ℓ values are lower and the peak shape is round rather than sharp when compared to the unsteady calculation. The displacement of the vortex path due to the influence of the blade causes the asymmetry in the solution. Blade loads are generally underestimated assuming steady state conditions.

Figure 16 compares the positive and negative C_ℓ peak values of the experiment to the computed values. The experimental values are shown to be considerably less than the computed values; however, both experimental and computed results show the negative C_ℓ peak to be smaller than the positive.

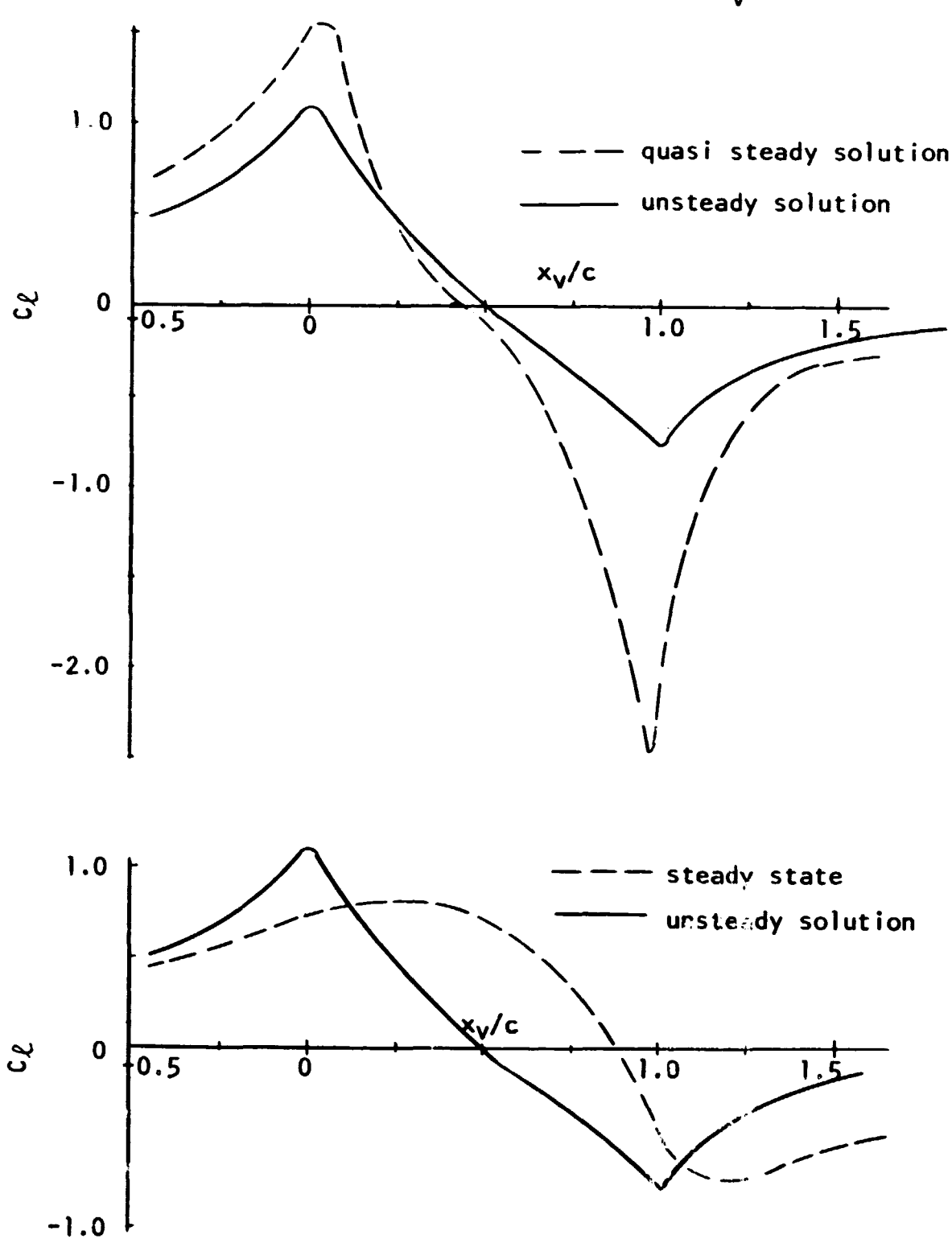

Figure 15 Effect of Quasi Steady and Steady State Assumptions

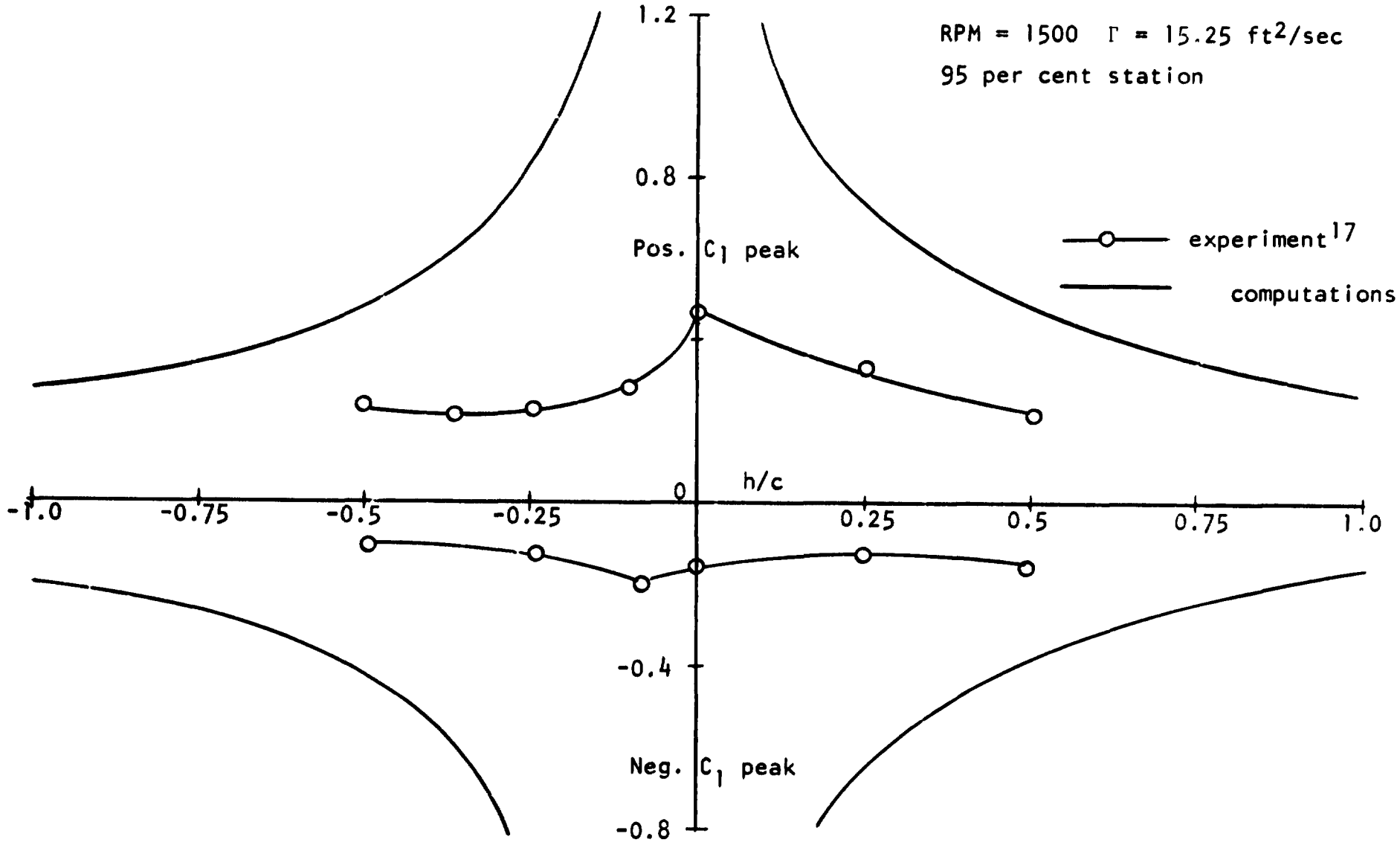

Figure 16 Typical comparison of Computed and Experimental C_l Peak Values

The total variation of C_ℓ through the vortex, ΔC_ℓ, plotted against h/c for constant Γ_v/Vc ratios is shown in Figure 17. The value of ΔC_ℓ increases with increasing vortex strength and with decreasing magnitudes of h/c. When ΔC_ℓ is compared for the same positive and negative h/c value, the negative value gives a greater ΔC_ℓ. This asymmetry is due to the unequal resultant velocity and angle of attack experienced by the blade as the vortex passes above or below the blade. It is also due to the displacement of the vortex path away from the blade for positive h/c values and toward the blade for negative values.

Figure 18a is a cross plot of Figure 17 where Γ_v/Vc is the independent variable. Experimental results for the 95 per cent radius station are included in the figure. It is clear that the experimental ΔC_ℓ magnitudes are well below those predicted.

The disagreement in the magnitude of the C_ℓ values can be explained. The most likely cause is the highly three-dimensional nature of the flow near the blade tip where Surendraiah's data was taken. Figure 18b presents the data for the 85 per cent station (further from the tip) where the ΔC_ℓ values are higher.

In order to obtain an approximate correction for three-dimensional effects, the spanwise C_ℓ distribution on a two bladed rotor at an arbitrary pitch angle is found using the vortex theory of propellers as given by McCormick [12]. The section lift coefficient at a spanwise

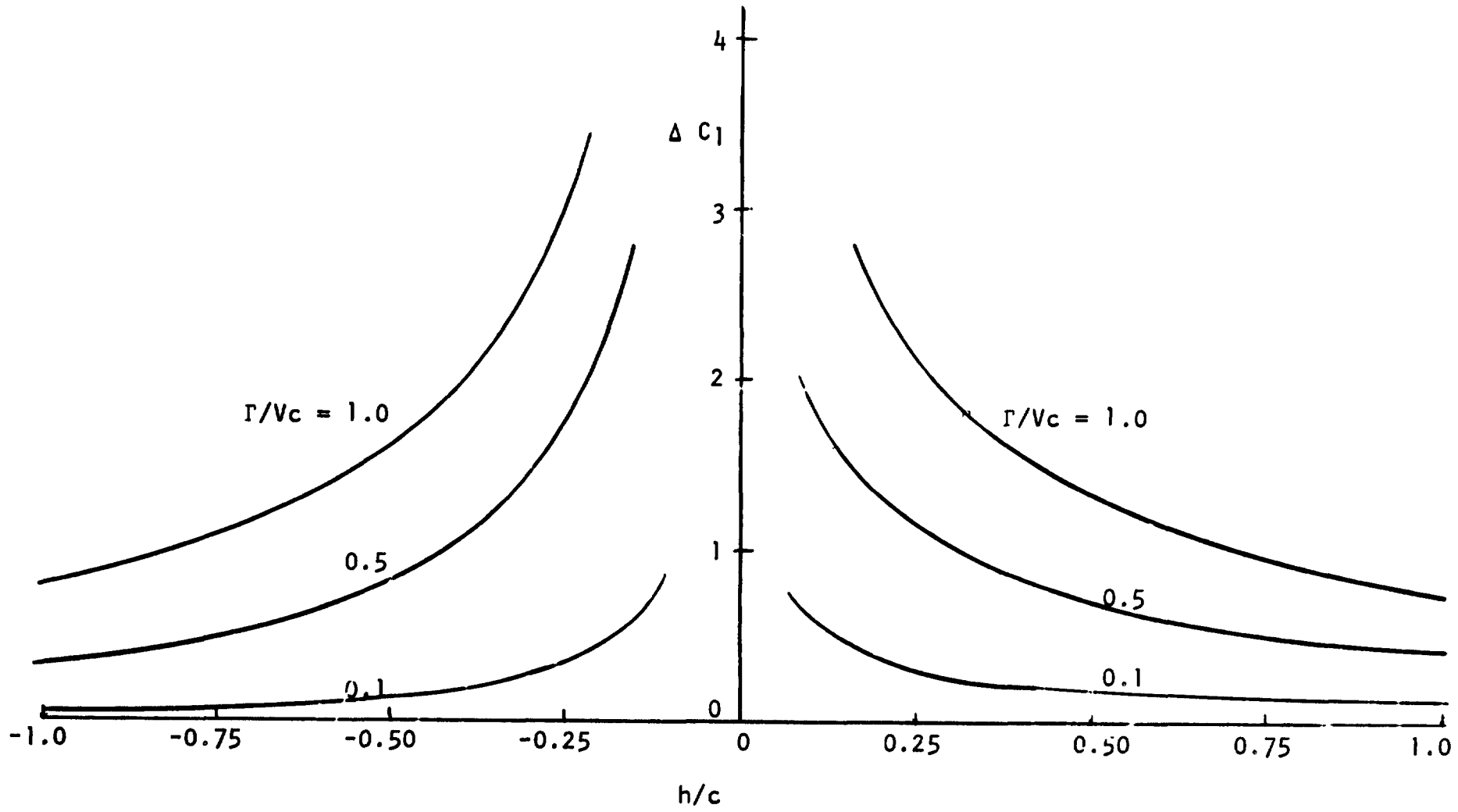

Figure 17 Computed ΔC_l in Vortex Interaction for constant Γ/Vc Ratios

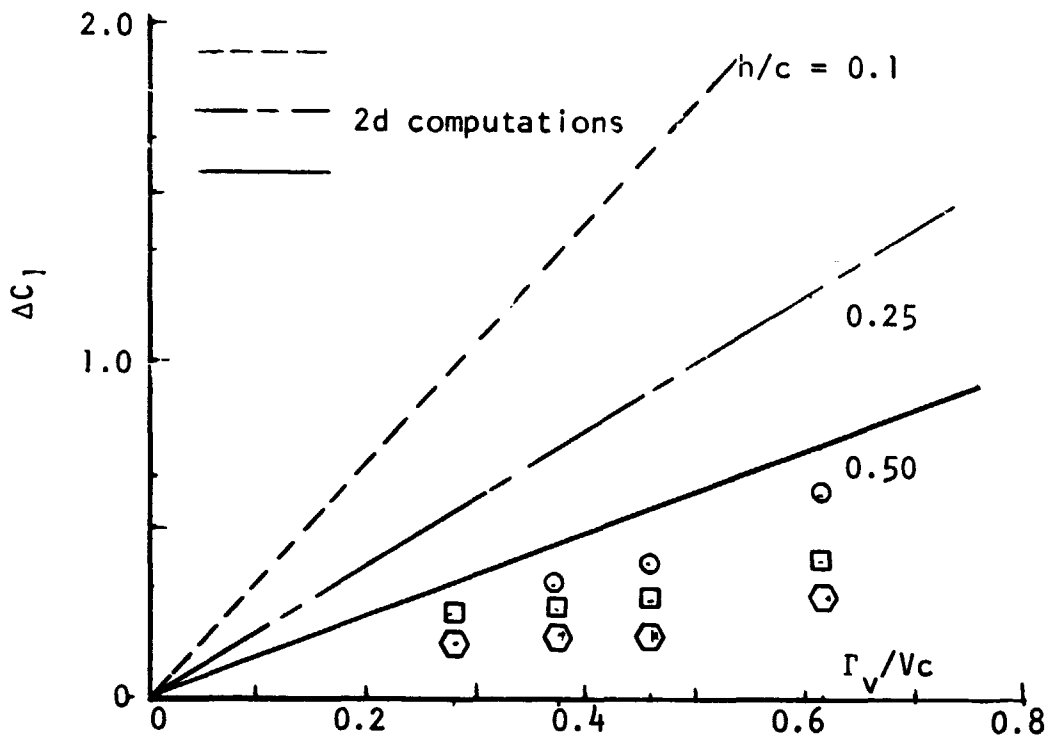

Figure 18a Computed ΔC_l for constant h/c ratios and Experimental Results at 95% Station

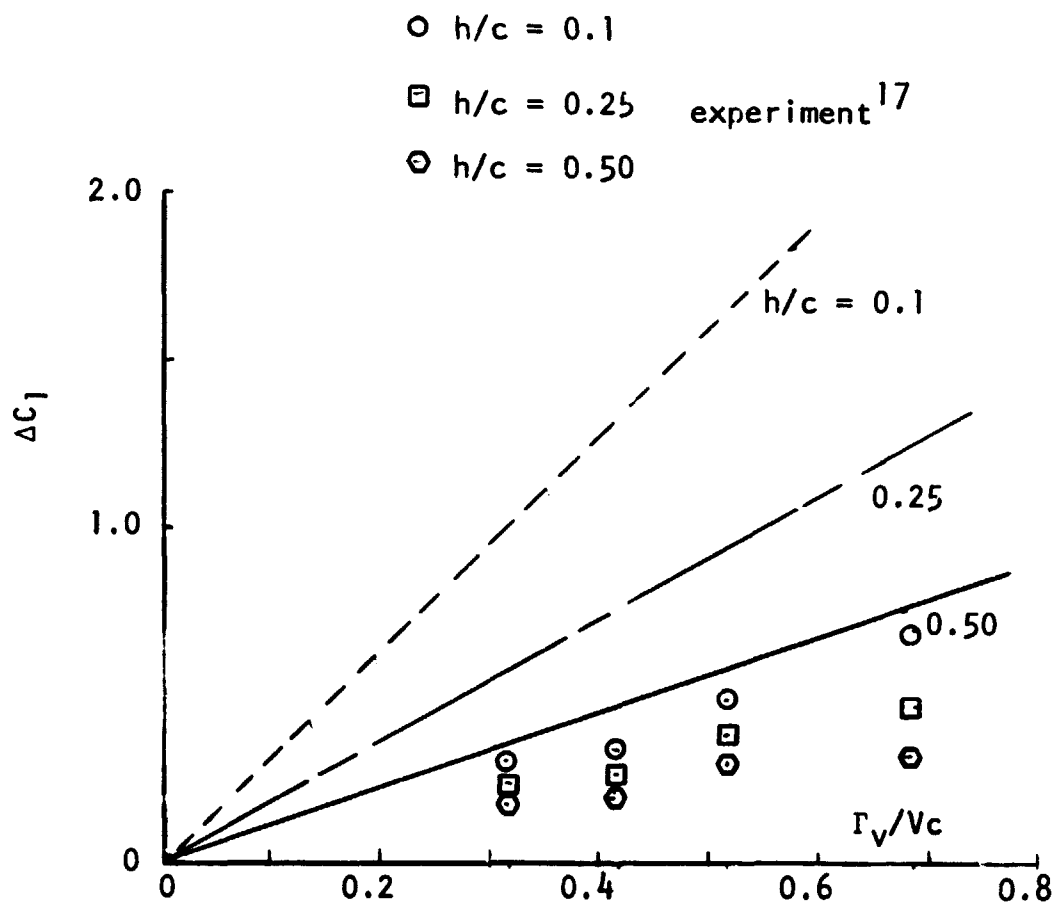

Figure 18b Computed ΔC_l for constant h/c ratios and Experimental Results at 85% Station

station is expressed in terms of the blade pitch angle, β, the downwash induced angle of attack, α_i, and the lift curve slope, a_o, as:

$$C_\ell = a_o (\beta - \alpha_i)$$

For the infinite aspect ratio case, α_i is zero and the ratio of C_ℓ to the two-dimensional value at a spanwise station becomes:

$$C_\ell / C_{\ell 2d} = 1 - \alpha_i/\beta \qquad (31)$$

The approximate α_i is expressed in terms of the rotor solidity, σ, the spanwise position, x, and the Prandtl tip loss factor, F, for the statically operating rotor as:

$$\alpha_i = 1/2[-\sigma a_o/8xF + ((\sigma a_o/8xF)^2 + \sigma a_o \beta/2xF)^{1/2}]$$

The tip loss factor may be calculated given the number of blades, B, and the pitch angle at the tip, β_T, as:

$$F = 2/\pi \cos^{-1} \exp\{-B(1-x)/2\sin\beta_T\}$$

Calculating the C_ℓ ratio of equation 31 for the 85 and 95 per cent stations:

$$\text{at } 95\% \quad C_\ell/C_{\ell^2 d} = 0.396$$

$$\text{at } 85\% \quad C_\ell/C_{\ell^2 d} = 0.460$$

Considering the tip effects, the computed two-dimensional results should differ from the experimental values by a factor of 2.5 at the 95 per cent station and 2.2 at the 85 per cent station. Figures 19a and b compare the theory to the experiment with the tip loss correction included. Much more satisfactory agreement is obtained for h/c of 0.25 and 0.50, but the predicted results for h/c of 0.1 are well above the experimental values. Since Surendraiah's results apply to a vortex whose core radius is 20 per cent of the blade chord, results using a potential vortex model for an h/c of 0.1 are questionable.

Another contributing factor to the three- dimensionality of the flow is the high advance ratio at which the rotor was operated. The

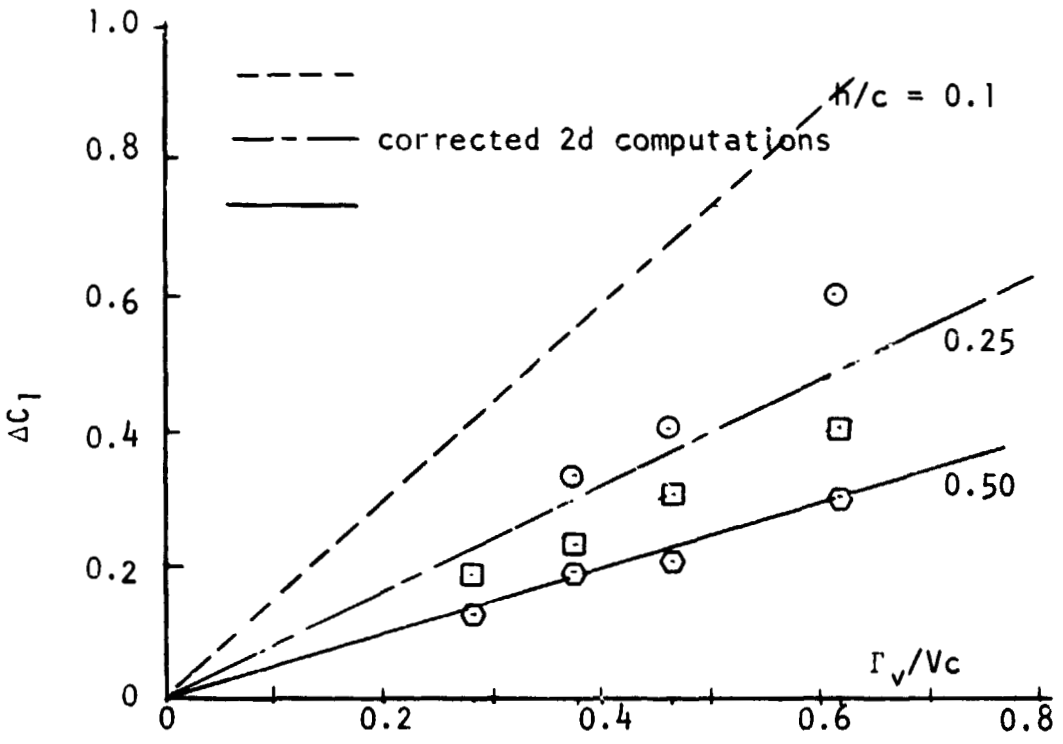

Figure 19a Computed ΔC_l Corrected for Tip Losses at 95% Station

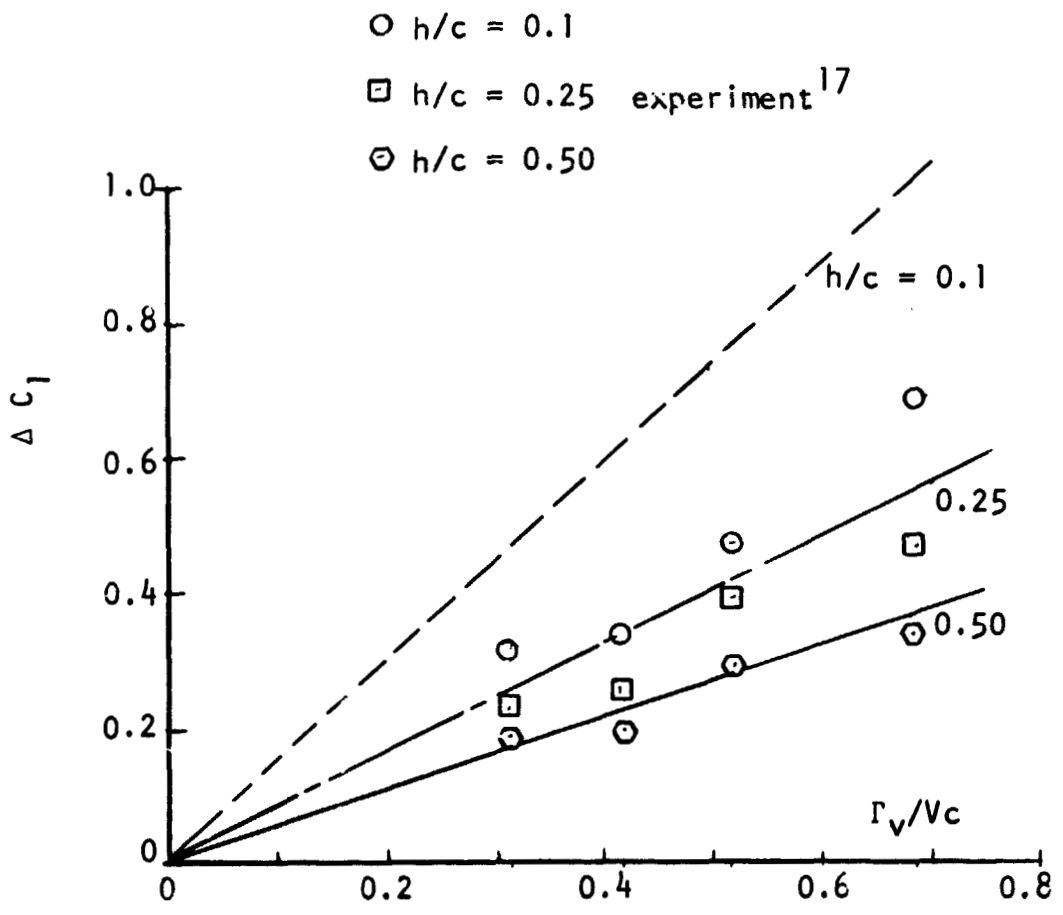

Figure 19b Computed ΔC_l Corrected for Tip Losses at 85% Station

vortex was generated using a 110 ft/sec tunnel velocity in the direction of the vortex axis. This velocity is parallel to the blade span for the 90 degree intersection angle and causes a cross flow pattern on the blade. The rotational velocity, when combined with the tunnel velocity, gives a resultant flow which is directed 29 degrees to the blade at 2000 RPM and 36 degrees at 1500 RPM. The blade is effectively swept forward during the interaction. The large angles of the flow relative to the chordwise pressure sensors give reason to question chordwise pressure distribution measurements, particularly near the tip.

The perfect fluid assumption used in the theory is another source of error. The maximum vortex induced angle of attack during the interaction is nearly 15 degrees. At the low Reynolds numbers used in the tests, approximately 1.5 to 2.2 x 10^5, flow separation may occur.

The theoretical results of Johnson[10] show agreement with Surendraiah's data except for the case of a δ of 90 degrees. Johnson's theory overpredicts the ΔC_ℓ magnitudes by a factor of two for this intersection angle. An infinite aspect ratio wing is used in his theory.

It is obvious from Figures 18 and 19 that the ΔC_ℓ is a linear

function of the nondimensional parameter Γ_v/Vc. This relationship is predicted by the analytical model and confirmed by Surendraiah's results. The total change of C_ℓ is expected to be proportional to Γ_v/Vc since the vortex-induced angle of attack also varies with this parameter. This can be shown by considering the velocity induced by a vortex on a blade at a distance h and x_v from the blade.

$$v_i = \Gamma_v/2\pi \, (h^2 + x_v^2)^{1/2}$$

If the induced velocity is assumed perpendicular to V, the vortex - induced angle of attack, for small angles, is given by:

$$\alpha_v = [\Gamma_v/2\pi \, (h^2 + x_v^2)^{1/2}]/V$$

The assumption is valid when the ratio of h/x_v is small and is the case when the vortex is not in close proximity to the blade. For a given x_v position, α_v varies as:

$$\alpha_v \propto \Gamma_v/Vh$$

Since constant values of h/c are used, h may be replaced by c in the proportionality to form the parameter Γ_v/Vc.

Figure 20 presents the time rate of change of ΔC_ℓ with h/c for constant Γ_v/c^2 ratios. The trends are similar to those of the ΔC_ℓ variation including the asymmetry, that is, a negative h/c gives a higher $\Delta C_\ell/\Delta T$ than the same positive value.

Figures 21a and b are cross plots of 20 where Γ_v/c^2 is the independent variable. Surendraiah's experimental results for the 95 per cent station are included in Figure 21a and the unpublished results for the 85 per cent station are presented in Figure 21b. A linear relationship between $\Delta C_\ell/\Delta T$ and the parameter Γ/c^2 for constant h/c is predicted by the analytical model. Only two values of Γ_v/c^2 were used in the experiment but, together with the origin, they do tend to confirm the linearity.

The time interval, ΔT, varies directly with c/V since the C_ℓ goes from a positive to negative peak in approximately one chord length. The relationship of $\Delta C_\ell/\Delta T$ to Γ_v/c^2 follows since ΔC_ℓ has been shown to be proportional to Γ_v/Vc.

The magnitudes of $\Delta C_\ell/\Delta T$ obtained experimentally are below that predicted by the same factor as the ΔC_ℓ values. This characteristic indicates the difference lies with the magnitude of ΔC_ℓ and not with the time interval. The tip loss correction factors are also applied to the $\Delta C_\ell/\Delta T$ values.

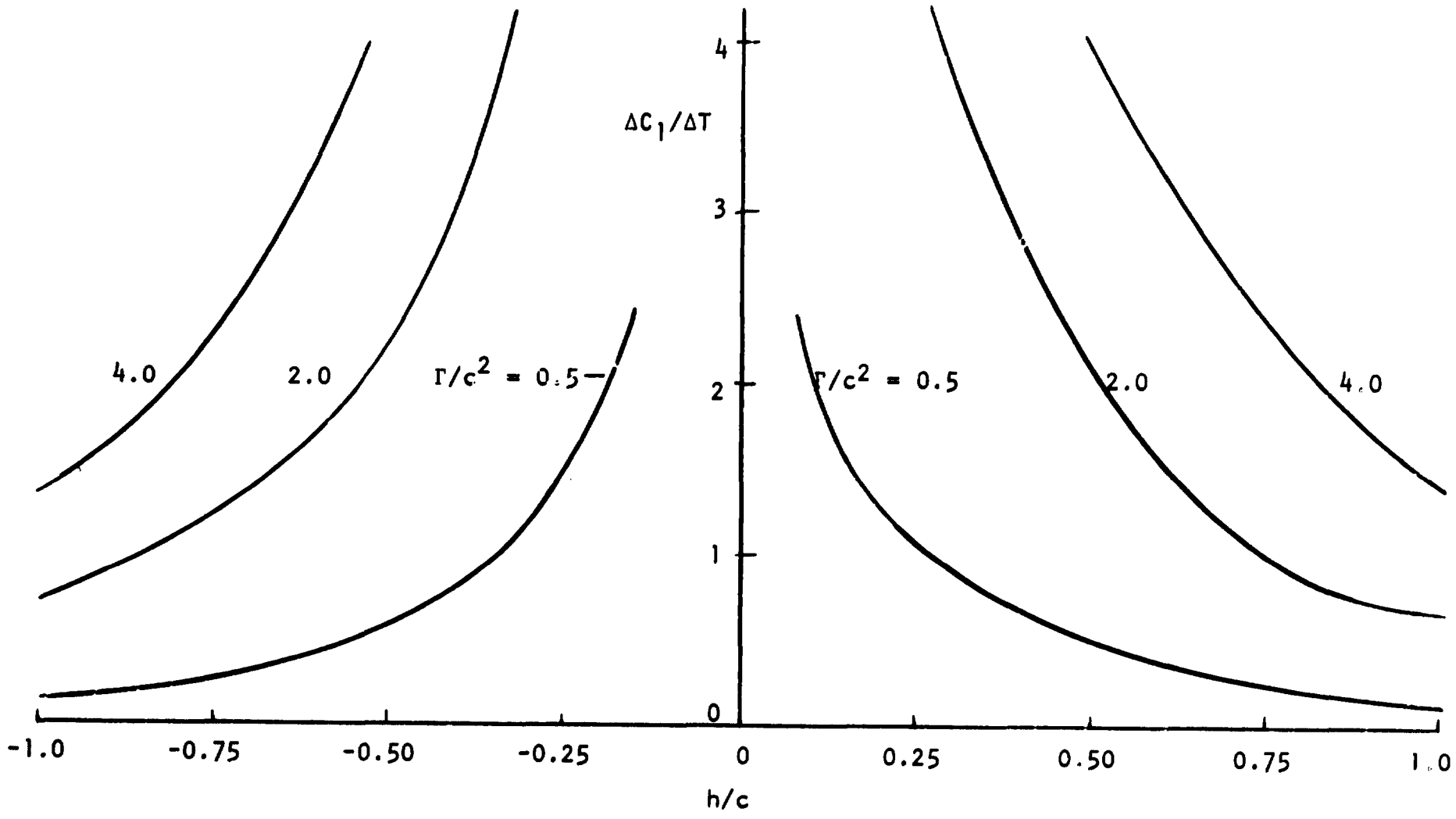

Figure 20 Time Rate of Change of ΔC_l in Vortex Interaction for constant Γ/c^2 Ratios

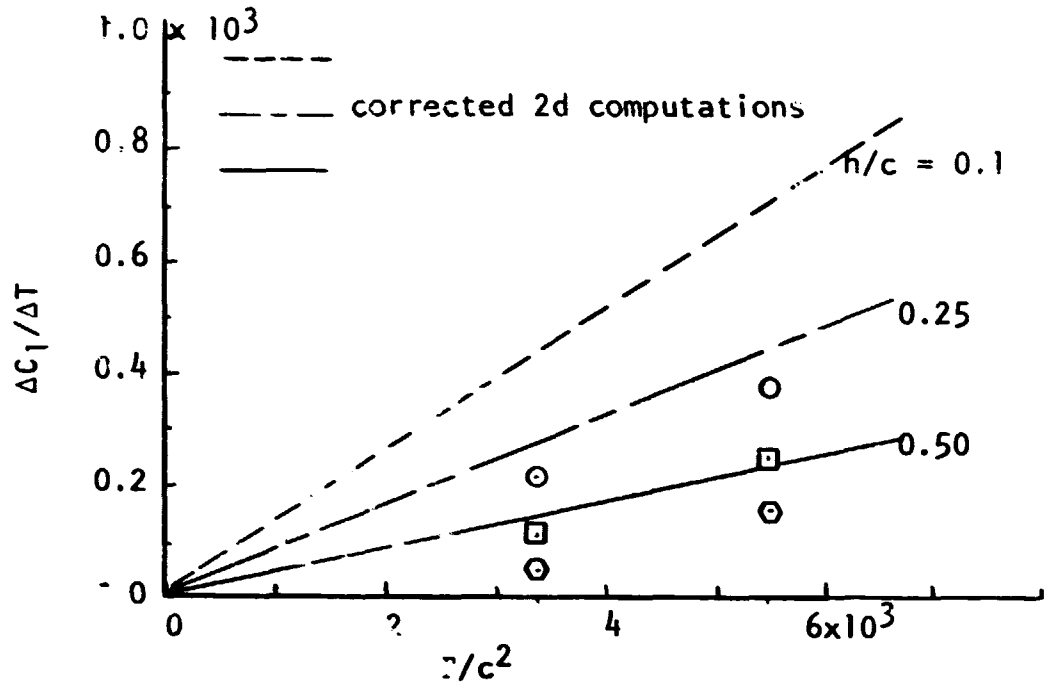

Figure 21a Computed $\Delta C_l/\Delta T$ Corrected for Tip Losses at 95% Station

○ h/c = 0.1

⊡ h/c = 0.25 experiment[17]

⊙ h/c = 0.50

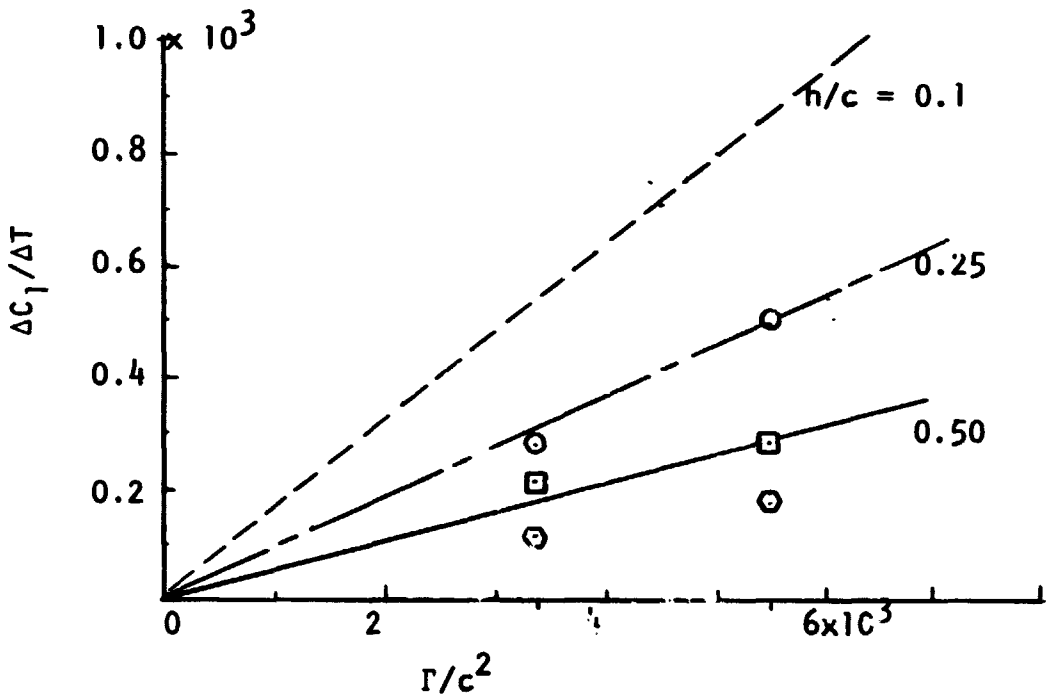

Figure 21b Computed $\Delta C_l/\Delta T$ Corrected for Tip Losses at 85% Station

VII. CONCLUSIONS

A numerical method for the computation of unsteady aerodynamic forces on a thin airfoil has been developed. The method has been compared to the linear theories of Theodorsen for an oscillating airfoil and Wagner for an impulsively started airfoil and satisfactory agreement obtained.

The numerical method has been applied to the vortex interaction problem by calculating the section lift coefficient as a potential vortex passes near an airfoil representing a helicopter blade section. The calculated results were compared with experimental measurements and the following conclusions reached.

1. The investigation proves the feasibility of a numerical method to predict the unsteady forces on an airfoil. The method uses discrete point vortices to represent the airfoil and wake.

2. In blade-vortex interactions, the shape of the C_ℓ variation as the blade passes near a vortex which is computed by the numerical model is similar

to that obtained experimentally. The computed time interval between peak C_ℓ values is in agreement with experimental measurements.

3. The maximum difference in section lift coefficient as a blade passes through a vortex varies directly with the vortex strength and inversely with the velocity and blade chord for a given ratio of blade-vortex separation distance to chord.

4. The time rate of change of the maximum difference in C_ℓ is a linear function of the ratio of vortex strength to the square of the blade chord for a given ratio of blade-vortex separation distance to chord.

5. Steady state or quasi steady assumptions are inadequate to predict the unsteady nature of the lift fluctuation during blade-vortex interaction.

6. Caution should be exercised in applying the two-dimensional model to the blade-vortex interaction problem, particularly in the vicinity of the blade tip. The blade loads are generally overestimated by the numerical solution when compared to experimental measurements. Satisfactory agreement is obtained by correcting the two-dimensional results for tip effects considering blade-vortex separation distances greater than the experimental vortex core radius.

7. The establishment of a long or semi-infinite wake is not required for agreement of the numerical calculations with the Theodorsen function. Agreement in phase and magnitude is obtained during the first cycle of oscillation for reduced frequencies from zero through ten.

8. In a numerical solution of unsteady airfoil

problems, the interval between successive time steps must be sufficiently small for accurate results. Periodic lift fluctuations require 60 time steps per cycle for agreement with Theodorsen within 8 per cent at a reduced frequency of ten. The error is less at lower reduced frequencies. Impulsive start problems require infinitesimal time increments at the instant of start but intervals which give a 1/10 chord shed vortex spacing will provide satisfactory agreement to the Wagner function 0.15 chord lengths after the start.

9. In general, the instantaneous chordwise pressure distribution for an airfoil in unsteady motion differs significantly from the steady state distribution.

REFERENCES

1. Bisplinghoff, R. L., Ashley, H., and Halfman, R. L., Aeroelasticity, 2nd Printing, Addison-Wesley Publishing Co., Reading, Mass., 1957, pp. 251-293.

2. Degelman, L. O., "NUM-2 Simultaneous Equations," Aug. 1968, The Pennsylvania State University, Department of Architectural Engineering.

3. Djojodihardjo, R. H., and Widnall, S. F., "A Numerical Method for the Calculation of Nonlinear, Unsteady Lifting Potential Flow Problems," AIAA Journal, Vol. 7, No. 10, October 1969, p. 2007.

4. Durand, W. F., Aerodynamic Theory, Division E, Section 8, 1st Edition, Vol. II, Dover Publications, New York, 1963, p. 99.

5. Giesing, J. P., "Unsteady Two-Dimensional Potential Flow with Lift," Douglas Aircraft Company Report No. LB-32144, March 1965.

6. James, R. M., "On the Remarkable Accuracy of the Vortex Lattice Discretization in Thin Wing Theory," Douglas Aircraft Company Report No. DAC 67211, February 1969.

7. Johnson, W., "A Lifting Surface Solution for Vortex Induced Airloads and Its Application to Rotary Wing Airloads Calculations," ASRL TR 153-2, M.I.T. Aeroelastic and Structures Research Lab., April 1970.

8. Johnson, W., "A Comparison Between Experimental Data and a Lifting Surface Theory Calculation of Vortex Induced Loads," ASRL TR 153-3, M.I.T. Aeroelastic and Structures Research Lab., August 1970.

9. Jones, W. P., and Rao, B. M., "Wing-Vortex Interaction," January 1970, Texas Engineering Experiment Station, Texas A & M University.

10. von Karman, T. and Sears, W. R., "Airfoil Theory for Non-Uniform Motion," Journal of the Aeronautical Sciences, Vol. 5, No. 10, August 1938, pp. 379-390.

11. Kfoury, Dennis J., "A Routine Method for the Calculation of Aerodynamic Roads on a Wing in the Vicinity of Infinite Vortices," ASRL TR 133-2, M.I.T. Aeroelastic and Structures Research Lab., May 1966.

12. McCormick, B. W., Aerodynamics of V/STOL Flight, Academic Press, New York, 1967, pp. 82-87.

13. Piziali, R. A., "Method for the Solution of the Aeroelastic Response Problem for Rotating Wings," Journal of Sound and Vibration, Vol. 4, No. 3, November 1966, pp. 445-486.

14. Sears, W. R., "Operational Methods in the Theory of Airfoils in Non-Uniform Motion," Journal of the Franklin Institute, Vol. 230, No. 1, July 1940, pp. 95-111.

15. Simons, I. A., "Some Aspects of Blade-Vortex Interaction on Helicopters in Forward Flight," Journal of Sound and Vibration, Vol. 4, No. 3, November 1966, pp. 268-281.

16. Spurck, J., "Measurements of Aerodynamic Coefficients of Oscillating Airfoils in the Wind Tunnel and Comparison with the Theory," LB 31959, Douglas Aircraft Company Report, Jan. 1964.

17. Surendraiah, M., "An Experimental Study of Rotor Blade-Vortex Interaction," M.S. Thesis, December 1969, Department of Aerospace Engineering, The Pennsylvania State University.

18. Theodorsen, Th., "General Theory of Aerodynamic Instability and the Mechanism of Flutter," NACA Report No. 496, 1940.

19. Widnall, S., "Helicopter Noise Due to Blade-Vortex Interaction," Department of Aeronautics and Astronautics, M.I.T., 1970

APPENDIX

Use of the Computer Program

The program has comment cards at the beginning to explain most of the input variables but some clarification is needed in certain cases.

First Data Card

N (format I5) - number of vortices to be placed on mean camber line.

MCHECK, NAUX, MREV, NSQ (all format I5) - parameters used in the routine to solve the simultaneous equations, explained in reference (2).

MPRINT (format I5) - equals 1 if user wants γ distribution printed for each time step. If left blank, only resulting C_ℓ will be printed.

Second Data Card

CHRD (format F10.3) - chord length of blade.

VEL (format F10.3) - free stream velocity.

W (format F10.3) - frequency of periodic vertical or rotational blade motions. If blade is rigid, make w = 2π and TO = 0.25 nd remove statement at end of deck "T = T + DELTT." For this case, AMAX is the fixed angle of attack.

AMAX (format F10.3) - amplitude of periodic angle of attack motion (radians).

AXIS (format F10.3) - position of the axis of rotation, measured downstream of mid chord in semichord lengths.

MT (format I10) - number of time steps.

Third Data Card

HMAXC (format F10.3) - amplitude of periodic plunging motion in chord lengths.

TO (format F10.8) - initial time, see notes on w above for fixed blade.

ZC (format F10.3) - initial vertical position of vortex, ho/c.

XC (format F10.3) - initial horizontal position of vortex, Xo/c.

GAMV (format F10.3) - strength of vortex.

Following N Data Cards - for cambered blade sections, the next N data cards are the z coordinates of the mean camber line at the control point positions. For zero camber, place N blank data cards here.

The program has been made flexible to consider both steady and unsteady problems. The simple steady state problem of a cambered thin airfoil at an angle of attack can be solved by using one time step. Periodic airfoil motions without the influence of the vortex are made by setting GAMV equal to zero. The impulsively started airfoil problem can be solved with a minor modification making the airfoil go from zero angle of attack to some value during the first time step and holding α constant from that time on.

The output is self-explanatory except for a few items. The vortex position x is in chord lengths from the mid-chord. The column entitled "mid-chord alpha" is the instantaneous angle of attack induced at the blade's mid-chord including the effect of the vortex.

It is noted that the dimension statement fixes the amount of storage space in use. At present, 10 is the maximum number of bound vortices and 150 is the maximum number of time steps.

PROGRAM FLOW CHART FOR AIRFOIL-VORTEX INTERACTION

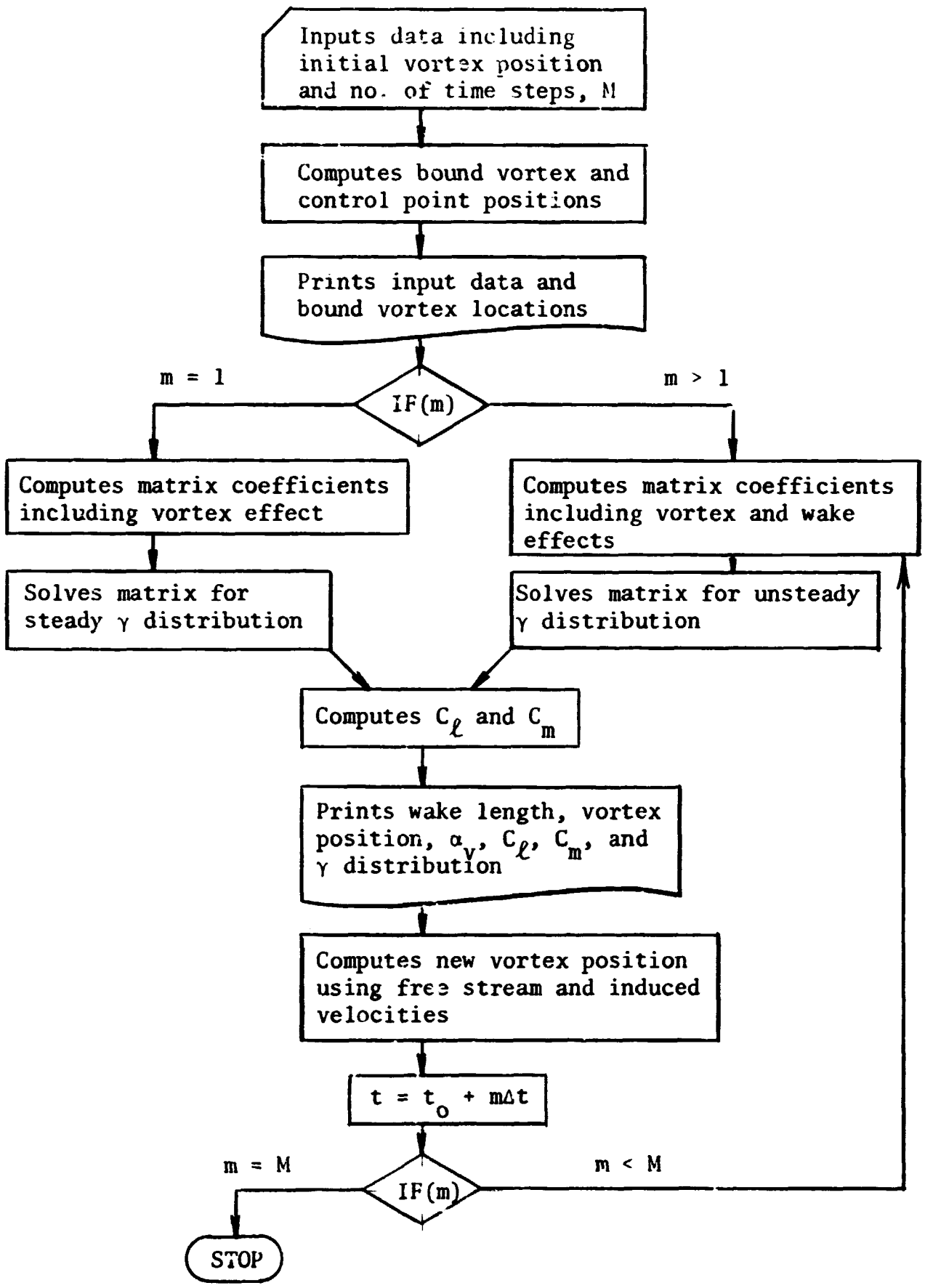

```
//              'P5865,T=100,R=4000,NASA','RUDHMAN W E'
// EXEC FWCLG
//SYSIN DD *
C      PROGRAM DEVELOPED TO SOLVE FOR VORTICITY DIST, COMPUTES THE
C      GEOMETRIC COEFFICIENTS A(I,J) AND SOLVES THE SIMUL EQUATIONS BY
C      BANACHIEWICZ-CROUT ALGORITHM WITH SUPPLEMENTAL ROUTINES.
C      READ IN INSTRUCTIONS.............
C       N=NUMBER OF EQUATIONS TO BE SOLVED.
C       CHRD = CHORD LENGTH OF AIRFOIL
C       VEL = FREE STREAM VELOCITY
C       W = FREQUENCY OF OSCILLATION
C       AMAX = MAX ANGLE OF ATTACK
C      AXIS = POSITION OF AXIS OF ROTATION
C       MT = NUMBER OF TIME STEPS
C       HMAXC = MAX VERTICAL OSCILLATION AMPLITUDE
C       TO = INITIAL TIME
C       ZC = INITIAL VALUE OF H/C
C       XC = INITIAL VALUE OF X/C
C       GAMV = PASSING VORTEX STRENGTH
C       Z(I) = MEAN CAMBER LINE COORDINATES AT THE CONTROL POINTS
      DIMENSION A(10,11),G(10,11),H(10,11),X(11),B(10,11),
     2Y(10),C(10),Z(10),D(150),GAM(150),DELTX(10),DELTZ(10),
     3 XN(10,150),GDX(10),VELIA(150), XI(10,150),ZII(10,150),
     3             ALPA(10),ALPAD(10),RVEL(10),CNA(10),XGAM(10,150)
    4 READ506,N,MCHECK,NAUX,MREV,NSQ,MPRINT
      IF(N) 800,800,406
  406 READ 751, CHRD,VEL,W,       AMAX,AXIS,MT
      READ 752, HMAXC,TO,ZC,XC,GAMV
      NP1=N+1
      NM1=N-1
      DO 2 I=1,N
      READ 799, Z(I)
    2 CONTINUE
      DO 55 I=1,N
      X(I) = (CHRD/(4.*N))+ (CHRD/N)*(I-1)
      C(I) = ((3.*CHRD)/(4.*N)) + (CHRD/N)*(I-1)
   55 CONTINUE
      RFREQ = (W*(CHRD/2.0))/VEL
      ZO = CHRD*ZC
      XO = CHRD*XC
      HMAX = CHRD*HMAXC
      PRINT 500, VEL,W,RFREQ,CHRD,GAMV,ZC,XC
      DELTT = CHRD/(30.*VEL)
      SPC = VEL*DELTT/CHRD
      PRINT 508, DELTT,SPC,AXIS
      DO 400 I=1,NM1
      DELTX(I)= X(I+1)-X(I)
      DELTZ(I)=Z(I+1)-Z(I)
  400 CONTINUE
      DELTX(N) = DELTX(NM1)
      DELTZ(N) = DELTZ(NM1)
      T = TO
      DO 902 M=1,MT
      MM1 = M-1
      MM2 = M-2
      S = MM1*DELTT*VEL/CHRD
      IF (M-2) 84,10,85
   84 PRINT 502
   10 DO 5 I=1,N
      DO 7 J=1,N
```

```
      IF(M-1) 83,83,81
   83 A(I,J) = 1.00 /(6.283*(C(I)-X(J)))
      GO TO 7
   81 A(I,J) = (1.00/(6.283*(C(I)-X(J))))+ (1.00/(6.283*(VEL*DELTT+
     2(CHRD-C(I)))))
    7 CONTINUE
    5 CONTINUE
      IF(M-2) 407,407,85
  407 DO 408 I=1,N
  408 PRINT 672,I,(A(I,J),J=1,N)
   85 ALPHA  = (AMAX/57.296)*SIN(W*T)
      ALPHD   =ALPHA   *57.296
      DRIVA = W*(AMAX/57.296)*COS(W*T)
      ALT=HMAX*SIN(W*T)
      DALT= W*HMAX*COS(W*T)
      VELIH= -DALT
      DO 401 I=1,N
      VELIA(I)=-((CHRD/2.00)*(AXIS+1.00)-C(I))*DRIVA
      ZI = ((CHRD/2.00)*(AXIS+1.0)-C(I))*ALPHA
      IF(M-1) 404,404,405
  404 XI(I,M) = XO - C(I)
      ZII(I,M) = ZO - ZI + Z(I)
      GO TO 409
  405 XI(I,M) = XI(I,MM1) + ((VEL+BVTVX+VWTX)*DELTT)
      ZII(I,M) = ZII(I,MM1) + ((BVTVZ+VWTZ)*DELTT)
  409 RSQ = ZII(I,M)*ZII(I,M) + XI(I,M)*XI(I,M)
      VX =-(-GAMV/6.283)*(ZII(I,M)/RSQ)
      VZ = (-GAMV/6.283)*(XI(I,M)/RSQ)
      ANG = (VZ/(VX+VEL))
      ALPA(I) = ATAN(ANG) + ALPHA
      ALPAD(I) = ALPA(I) * 57.296
      RVEL(I) = SQRT(VZ*VZ+(VEL+VX)*(VEL+VX))
  401 CONTINUE
   94 IF(M-2) 95,91,9
    9 DO 11 I=1,N
      SUMD = 0.00
      DO 3 LT=1,MM2
      D(LT)=(GAM(M-LT)-GAM(MM1-LT))/(6.283*(VEL*(LT+1)*DELTT+
     2(CHRD-C(I))))
      SUMD = D(LT)+SUMD
    3 CONTINUE
      A(I,NP1) = RVEL(I)*SIN(ALPA(I)-(DELTZ(I)/DELTX(I)))+(GAM(MM1)/
     2(6.283*(VEL*DELTT+(CHRD-C(I))))) -SUMD
     4+VELIA(I)+VELIH
   11 CONTINUE
      GO TO 15
   91 DO 93 I=1,N
      A(I,NP1) = RVEL(I)*SIN(ALPA(I)-(DELTZ(I)/DELTX(I)))
     3+GAM(1)/(6.283*(VEL*DELTT+(CHRD-C(I))))
     4+VELIA(I)+VELIH
   93 CONTINUE
      GO TO 15
   95 DO 12 I=1,N
      A(I,NP1) = RVEL(I)*SIN(ALPA(I)-(DELTZ(I)/DELTX(I)))
   12 CONTINUE
C  15 CARD 15 BEGINS THE ROUTINE TO COMPUTE THE VORTICITY DISTRIBUTION
C     BY SOLUTION OF THE SIMULTANEOUS EQUATIONS. THE OUTPUT IS GDX(I).
   86 GAM(M) = 0.00
      DO 13 I=1,N
      GAM(M) = GDX(I)+GAM(M)
```

```
      XN(I,M)=GDX(I)
   13 CONTINUE
      BVTVX = 0.00
      BVTVZ = 0.00
      DO 410 J=1,N
      VXI =(GDX(J)/6.283)*(ZII(J,M)/RSQ)
      VZI = -(GDX(J)/6.283)*(XI(J,M)/RSQ)
      BVTVX = VXI + BVTVX
      BVTVZ = VZI + BVTVZ
  410 CONTINUE
      SUMWX = 0.00
      SUMWZ = 0.00
      VWTZ = 0.00
      VWTX = 0.00
      ZW = ZII(N,M)
      IF(M-2) 413,414,415
  415 DO 411 LT = 1,MM2
      XW = XO - CHRD + (VEL*DELTT)*(M-LT-2)
      RSQW = XW*XW +ZW*ZW
      SUMWX = -((GAM(M-LT)-GAM(MM1-LT))*ZW/(6.283*RSQW))+SUMWX
      SUMWZ = -((GAM(M-LT)-GAM(MM1-LT))*XW/(6.283*RSQW))+SUMWZ
  411 CONTINUE
  414 XW = XO - CHRD +(VEL*DELTT)*MM2
      RSQW = XW*XW + ZW*ZW
      VWTX = -((GAM(M)-GAM(MM1))*ZW/(6.283 * RSQW)) +SUMWX
      VWTZ = -((GAM(M)-GAM(MM1))*XW/(6.283*RSQW))+SUMWZ
  413 CL     = (2.00*GAM(M))/(VEL*CHRD)
      XGAM(1,M) = XN(1,M)*((CHRD/2.)*(1.+AXIS)-X(1))
      DO 17 I=2,N
      XGAM(I,M) = XN(I,M)*((CHRD/2.)*(1.+AXIS)-X(I))+XGAM(I-1 ,M)
   17 CONTINUE
      ELM =  2.*XGAM(N,M)/(VEL*CHRD*CHRD)
      IF(M-1)900,900,72
   72 CNA(1) = (XN(1,M)-XN(1,MM1))/DELTT
      DO 420 I=2,N
      CNA(I) = ((XN(I,M)-XN(I,MM1))/DELTT)+CNA(I-1)
  420 CONTINUE
      CN =0.00
      CMB = 0.00
      DO 14 I=1,N
      CN = CNA(I)*DELTX(I) + CN
      CMB = ((XGAM(I,M)-XGAM(I,MM1))/DELTT)*DELTX(I) +CMB
   14 CONTINUE
      ELMI = (2./(VEL*VEL*CHRD*CHRD))*CMB
      CNL    =  (2.00*CN)/(VEL*CHRD*VEL)
      CM = ELM +ELMI
      TOT = CL +CNL
      GO TO 901
  900 I=N/2
      XR = XI(I,M)/CHRD
      ZR = ZII(I,M)/CHRD
      PRINT 501
      PRINT 510, C(1),C(2),C(3),C(4),C(5),C(6)
      PRINT 503,X(1),X(2),X(3), X(4),X(5),X(6)
      PRINT 505, M,S,XR,ZR,ALPAD(I),ELM,CL
      PRINT 507, GDX(1),GDX(2),GDX(3),GDX(4),GDX(5),GDX(6)
      GO TO 902
  901 I=N/2
      XR = XI(I,M)/CHRD
      ZR = ZII(I,M)/CHRD
```

```
      PRINT 504,M,S,   XR   , ZR        ,ALPAD(I), CM,CL    ,CNL    ,TOT
      PRINT 509, GDX(1),GDX(2),GDX(3),GDX(4),GDX(5),GDX(6)
  902 CONTINUE
      GO TO 4
  500 FORMAT (1H1,9X,10HVELOCITY =,F10.2,5X,6HFREQ =,F10.3,5X,         8H
     2R FREQ =,F6.3,4X,6HCHRD =,F6.3,5X,26HVORTEX STRENGTH (FT-SEC) =,F1
     30.3//9X,11HINITIAL Z =,F10.3,7X,11HINITIAL X =,F10.3)
  501 FORMAT(1H1,7X,6HNUMBER,11X,2HWL,  6X,6HVORTEX,6X,6HVORTEX,3X,
     29HMID CHORD,4X,8HMOMENT C,7X,5HGAMMA,4X,8HTIME DEP,6X,5HTOTAL/
     335X,6HPOS. X,6X,6HPOS. Z,3X,5HALPHA,8X,7HAT AXIS,8X,6HLIFT C,4X,
     46HLIFT C,6X,6HLIFT C/)
  502 FORMAT(1HO,15X,15HORIGINAL MATRIX)
  510 FORMAT(1H ,'CONTROL POINT LOCATIONS.',6F10.5)
  503 FORMAT(1H ,'POINT VORTEX STRENGTHS AT POSITIONS.',6F10.5,//)
  504 FORMAT(1H ,I10,F18.8,7F12.5)
  505 FORMAT(1H ,I10,F18.5,5F12.5)
  506 FORMAT(615)
  507 FORMAT(1H ,33X,5F15.5)
  508 FORMAT (1H , 3X,'DELTT =',F15.5,5X,'WAKE ELEMENT SPACING =',F15.5,
     25X,'AXIS POSITION =',F10.3,' SEMI-CHORDS',/)
  509 FORMAT(1H ,33X,5F15.5)
  672 FORMAT(1HO,I5,4X,12F10.5/(10X,12F10.5))
  680   FORMAT(1H ,7X,'GDX',I2,'=',F15.5,6X,F14.5,12X,F15.5,10X,F15.5,
     210X,F8.4)
  751 FORMAT (F10.5,4F10.3,I10)
  752 FORMAT (F10.3, F10.8,3F10.3)
  799 FORMAT (F10.4)
  800 STOP
      END
/*
//DATA.INPUT DD *
    6
  1.00      2.00      6.283      0.00       0.50              50
  0.00      0.25       1.0         -2.50     2.00



/*
```